

Electron-impact excitation of the $D^3\Sigma_u^+$ and $c'_4{}^1\Sigma_u^+$ Rydberg states of N_2

Albert R. Filippelli, S. Chung, and Chun C. Lin

Department of Physics, University of Wisconsin, Madison, Wisconsin 53706

(Received 24 October 1983)

Absolute optical-emission excitation functions have been measured for the $D^3\Sigma_u^+ \rightarrow B^3\Pi_g$ fourth positive system bands ($0, v''$) with $v''=0,1,2,3,4,5,6$ and for the $c'_4{}^1\Sigma_u^+ \rightarrow a^1\Pi_g$ Gaydon-Herman singlet system bands ($0, v''$) with $v''=0,1,2,3,4,5$ produced by electron-impact excitation of the N_2 $X^1\Sigma_g^+(v=0)$ ground state, for incident electron energies ranging from threshold to 440 eV. We find that the $D \rightarrow B$ emission has a principal maximum at 14.1 ± 0.3 eV, a smaller maximum (83% of principal maximum) at 23 eV, and an E^{-3} energy dependence for incident electron energies $E > 65$ eV. Measurements over the energy range 13.5–31 eV indicate the $D \rightarrow B$ emission is unpolarized. The sum over v'' of the $D \rightarrow B$ ($0, v''$) optical-emission cross sections gives a maximum value 1.27×10^{-19} cm² for the apparent cross section for the $v=0$ vibrational level of the $D^3\Sigma_u^+$ state excited by electron collision with the N_2 $X^1\Sigma_g^+(v=0)$ ground state. The appearance of two maxima in the $D \rightarrow B$ optical emission is qualitatively confirmed by other experimental work. This point is discussed. For the $c'_4 \rightarrow a$ emission we find a single very broad maximum near 80 eV and for $E > 110$ eV an energy dependence described by the form $(C_1/E)\ln(E/C_2)$. The $c'_4 \rightarrow a$ optical-emission cross sections were obtained by extrapolating measurements to low pressure (< 0.1 mTorr) in order to account for the nonlinear pressure dependence of the $c'_4 \rightarrow a$ emission caused by absorption of the very intense $c'_4 \rightarrow X$ ($0,0$) band radiation. The sum over v'' of our measured optical-emission cross sections for the $c'_4 \rightarrow a$ ($0, v''$) bands has a maximum value 1.0×10^{-19} cm². This result, when combined with the absolute $c'_4 \rightarrow X$ ($0,0$) band-emission cross section of Zipf and McLaughlin and the $c'_4 \rightarrow X$ ($0,1$) cross section of Aarts and DeHeer, yields an upper bound of 0.006 for the $c'_4(0) \rightarrow a$ optical branching ratio, i.e., more than 99.4% of $c'_4{}^1\Sigma_u^+(v=0)$ molecules will decay to the ground state.

I. INTRODUCTION

The laboratory study of electron-impact excitation of the nitrogen molecule is useful for increasing our knowledge about the excited electronic states of the molecule, as well as for enhancing our ability to interpret optical emission from the earth's atmosphere.¹ Although numerous papers have been published on various aspects of the electron-impact excitation of N_2 , there are gaps in our knowledge, as well as inconsistent data, so that much still remains to be done. Most previous *optical method* studies of electron-impact excitation of N_2 have been concerned with lower-lying valence-type states, whereas in the present work we study the excitation of two higher-lying Rydberg-type states of N_2 . Our results have a bearing on the interpretation of optical emission from these lower-lying states.

In this paper, we report and discuss the results of our study, by the optical method, of the production of the $D^3\Sigma_u^+(v=0)$ and $c'_4{}^1\Sigma_u^+(v=0)$ states of N_2 by controlled electron collision with molecules in the lowest vibrational level of the singlet $X^1\Sigma_g^+$ ground state. Figure 1 shows the relevant energy levels and transitions. The $c'_4{}^1\Sigma_u^+$ state is known² to be the first member of a Rydberg series of *singlet* states converging to the $X^2\Sigma_g^+$ ground state of N_2^+ , and the $D^3\Sigma_u^+$ state is identified³ as the first member of a Rydberg series of *triplet* states, also

converging to the $X^2\Sigma_g^+$ ground state of N_2^+ . Both the $D^3\Sigma_u^+$ and the $c'_4{}^1\Sigma_u^+$ states have been assigned the same molecular-orbital configuration $(1\sigma_g)^2(1\sigma_u)^2(2\sigma_g)^2(2\sigma_u)^2(1\pi_u)^4(3\sigma_g)(4p\sigma_u)$. Here, the designation $4p$ refers to the quantum numbers for the limiting united atom. In the early literature, the $c'_4{}^1\Sigma_u^+(v=0)$ state was denoted $p^1\Sigma_u^+$.

An early experimental work on electron-impact excitation of the N_2 $c'_4{}^1\Sigma_u^+(v=0)$ state using the optical method is that reported by Aarts and DeHeer,⁴ who measured the absolute optical-emission cross section for the $c'_4{}^1\Sigma_u^+ \rightarrow X^1\Sigma_g^+$ ($0,1$) band at 981 Å, over the electron energy range 60–2000 eV, and for the $c'_4{}^1\Sigma_u^+ \rightarrow a^1\Pi_g$ ($0,0$) band at 2827 Å, over the range 100–2000 eV. See Fig. 1(b). More recently, Zipf and McLaughlin⁵ have made absolute optical-emission cross-section measurements for a number of bands of the $c'_4{}^1\Sigma_u^+(v') \rightarrow X^1\Sigma_g^+(v'')$ system for $0 \leq v' \leq 7$. These $c'_4 \rightarrow X$ bands all occur in the extreme-uv spectral region. Most recently, Huschilt *et al.*⁶ again using the optical method with crossed electron and molecule beams, have made measurements of the energy dependence of the apparent excitation function for the $v'=0$ level of $c'_4{}^1\Sigma_u^+$, using the ($0,0$) and ($0,1$) bands of the $c'_4 \rightarrow X$ system. Our work, which is based upon the $c'_4{}^1\Sigma_u^+ \rightarrow a^1\Pi_g$ band system in the near-uv spectral region, will supplement the work of these other investigators.

The previously published optical method investigations of electron-impact excitation of the $D^3\Sigma_u^+$ state have been those of Freund⁷ who studied the energy dependence of the $D^3\Sigma_u^+ \rightarrow B^3\Pi_g(0,1)$ band and of Skubenich and Zapesochny,⁸ who reported absolute measurements of the cross section for direct electron-impact excitation of the $D^3\Sigma_u^+$ state. Our results for the electron-impact excitation of the D state differ substantially from the results of Refs. 7 and 8. These differences are discussed in Sec. V.

II. EXPERIMENT

A. Optical method

In the *optical method* for study of the production of some excited rovibronic state j by electron collision with ground-state molecules, one sends a collimated, approximately monoenergetic electron beam through the target gas and measures the intensity and polarization of the radiation emitted by state j molecules; the gas density and electron-beam current are small enough that all secondary collision processes which can affect the excited-state population are negligible. Such secondary processes include the following. (a) Collisions of excited molecules with electrons or other molecules. (b) Forward inelastic scattering of primary beam electrons and forward ejection of electrons in ionizing collisions. Such collisions will broaden the energy spread of electrons traveling through the volume of gas from which light is gathered and consequently introduce distortion in the energy dependence of the cross section, as determined experimentally. (c) Back-

scattering, both elastic and inelastic, or primary beam electrons and backward ejection of electrons produced in ionizing collisions. In addition to contributing a larger energy spread as in (b), some of the backscattered primary beam electrons have a second chance of exciting a target molecule in the volume studied. We assume that the natural radiative lifetime τ_j of state j molecules (as well as the lifetime τ_k of higher-lying states k which can decay into state j) to be very short with respect to the time ($\sim 25 \mu\text{sec}$) required for a molecule to travel from the axis of the electron beam to the surface of the surrounding experimental apparatus. For the case in which the excited state j can make an allowed radiative transition to the ground state X , we also assume the gas density is sufficiently low that absorption of the $j \rightarrow X$ radiation causes a negligibly small change in the density of j -state molecules. We also assume a negligible effect due to secondary and reflected electrons from the metal surfaces of the apparatus. Under these assumptions above, the only significant processes which will produce N_2 molecules in excited state j are (1) direct electron-ground-state-molecule collisions and (2) spontaneous radiative decay of higher-lying states k into state j (cascade). In the steady state, the rate of production of state- j molecules by processes (1) and (2) above is balanced by the rate of loss of state- j molecules due to radiative decay. Then, in the steady state we have

$$Q_{\text{dir}}(j) = \frac{1}{(I/e)\rho_g} \left[\frac{\mathcal{N}_j}{\tau_j} - \sum_k \left[\frac{\mathcal{N}_k}{\tau_k} \right] \Gamma_{kj} \right], \quad (1)$$

where $Q_{\text{dir}}(j)$ is the cross section for direct production of the rovibronic state j by electron collision with a ground-state molecule, ρ_g is the target gas density, I is the electron-beam current, e is the absolute value of the electron charge, \mathcal{N}_j is the steady-state number of state j molecules *per unit length* in the beam direction, τ_j is the natural lifetime of state j , and k is a label referring to higher-lying rovibronic states which can radiatively decay into the state j with optical branching ratio Γ_{kj} . Equation (1) has been written in terms of the excited-state densities \mathcal{N}_j and \mathcal{N}_k because these quantities are most directly related to what we measure in the laboratory, viz., optical-emission intensities per unit beam length. In terms of *optical-emission cross sections* Q_{opt} , Eq. (1) for $Q_{\text{dir}}(j)$ becomes

$$Q_{\text{dir}}(j) = \sum_i Q_{\text{opt}}(j \rightarrow i) - \sum_k Q_{\text{opt}}(k \rightarrow j), \quad (2)$$

where

$$Q_{\text{opt}}(k \rightarrow j) \equiv \left[\frac{\mathcal{N}_k}{(I/e)\rho_g\tau_k} \right] \Gamma_{kj}. \quad (3)$$

Physically, $Q_{\text{opt}}(k \rightarrow j)$ is the number of $k \rightarrow j$ photons per second emitted per unit beam length, per unit electron flux, and per unit target gas density. In going from Eq. (1) to (2), we have inserted a unit factor $\sum_i \Gamma_{ji}$ in the first term on the right-hand side of Eq. (1), where the label i refers to all lower-lying states into which state j can decay.

In the present experiment, we could resolve some of the rotational components $j \rightarrow i$ of the $c'_4 \rightarrow a$ and $D \rightarrow B$

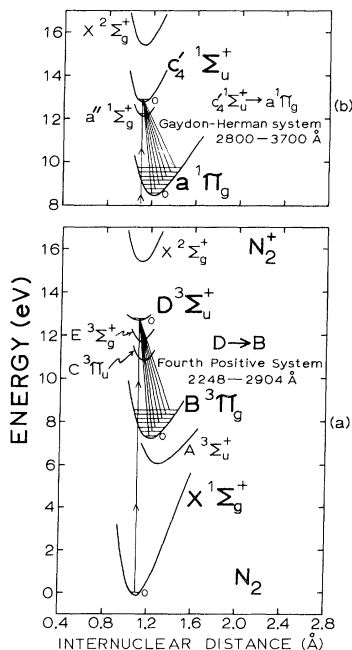


FIG. 1. Energy curves and associated transitions for electronic states of N_2 which are relevant to discussion of the results of the present work. For clarity, the curves for the excited triplet and singlet spin states are shown separately in (a) and (b), respectively.

molecular bands; however, no component $j \rightarrow i$ was sufficiently intense to be studied individually. Consequently, we instead measured the *sum* of the optical-emission cross sections $Q_{\text{opt}}(j \rightarrow i)$ for all the components $j \rightarrow i$ of a molecular band (v', v''). Denoting this molecular band-emission cross section by $Q_{\text{opt}}(v', v'')$, Eq. (2) becomes

$$Q_{\text{dir}}(v') = \sum_{v''} Q_{\text{opt}}(v', v'') - \sum_v Q_{\text{opt}}(v, v'), \quad (4)$$

where the sum on v'' is over all lower-lying vibrational levels of other electronic states into which c_4^1 or D decay and the sum on v is over all higher-lying vibrational levels of other electronic states which decay into c_4^1 or D . $Q_{\text{dir}}(v')$ is then the cross section for exciting, by electron impact, the entire set of rotational levels associated with the vibrational level v' of electronic state D or c_4^1 , averaged over the rotational state distribution for the electronic-vibrational ground state at 300 K. In this work, the optical-emission cross sections are determined by measuring the absolute intensity of the molecular band radiation emitted per unit beam length and per unit solid angle in a direction *perpendicular* to the direction of the electron beam.

B. Experimental apparatus

In our experiment, an approximately monoenergetic electron beam is generated by an electron gun operating in a chamber which has been evacuated to a pressure $< 10^{-8}$ Torr and then filled with research grade (total impurities specified to be < 6 ppm) N_2 gas to a pressure ≤ 10 mTorr. Figure 2 is a scale drawing of a section through the electron gun, containing the electron-gun axis XX' and the orthogonal axis OA of the external optics. The axes XX' and OA intersect inside the cylindrical part of the Faraday cup labeled 9, at a point P about 9.5 mm past the grounded electrode, labeled 8. Radiation from excited species in the approximately electric-field-free interior of the Faraday cup escapes through two symmetrically positioned, 2.5-mm-wide, 18.6-mm-high slots in the wall of the cylinder. The optical components in this experiment are arranged so that, in effect, we collect only radiation from a volume of space defined by two planes perpendicular to XX' , centered about the point P , and separated by Δx . This is illustrated in Fig. 3, which is a schematic diagram

of the entire apparatus. The relative positions of the various optical components are drawn to scale. The line CD is perpendicular to OA . The center of the first surface mirror M_2 (1-m radius of curvature) is placed on optical distance of 1 m from the point P , where XX' and OA intersect (see Fig. 2). The axis of mirror M_2 is rotated 3.6° away from the line CD and the monochromator is positioned so that the center of its entrance slit plane coincides with the unit-magnified image of point P , formed by M_2 . The monochromator is oriented so that light traveling along OA from XX' will emerge from the center of the monochromator exit slit. Because of the unit-magnification imaging of P onto the entrance slit, the separation Δx mentioned in regard to Fig. 2, is determined only by the smaller of e_2' and e_1 , where e_1 is the entrance slit width and e_2' is the width of the exit slit image which the monochromator forms at the location of e_1 . For the work reported here, $\Delta x \leq 0.61$ mm. The solid angle of collection Ω_c , for light gathered from the electron-beam-excited gas, was determined by the solid angle subtended at point P by the circular aperture S , located between M_1 and M_2 . For the work reported here, $\Omega_c \leq 7.09 \times 10^{-3}$ sr ($f/10.5$). An RCA C31034A photomultiplier tube (PMT) with GaAs photocathode cooled to -25°C was used with an electrometer to convert the photon flux from the monochromator to a proportional voltage, which was recorded on a strip chart or X-Y recorder.

The magnetically shielded⁹ electron gun (Fig. 2) was modeled after the pentode design of radio vacuum tubes, with the purpose of making the beam current almost independent of accelerating voltage (except for very low voltages), other voltages held fixed. Elements 1, 2, and 4 correspond to the control, screen, and suppressor grids, respectively. The additional element 3 was included to allow more freedom in controlling the beam diameter in the vicinity of point P . The potentials of elements 1, 2, 3, and 4 were referenced to the cathode K , to which the negative accelerating potential was applied. Ordinarily, we used $V_2 = 60$ V, $V_3 = 150$ V, and $V_4 = 0$ V. The potential of element 1, which was varied from 0 to -60 V with respect to K , was used to control the magnitude of the electron-beam current I collected by the Faraday cup (defined by elements 8, 9, and 11). The Faraday cup was made long with respect to its diameter to insure that a negligible (< 0.01 V/cm) field was generated in the vicini-

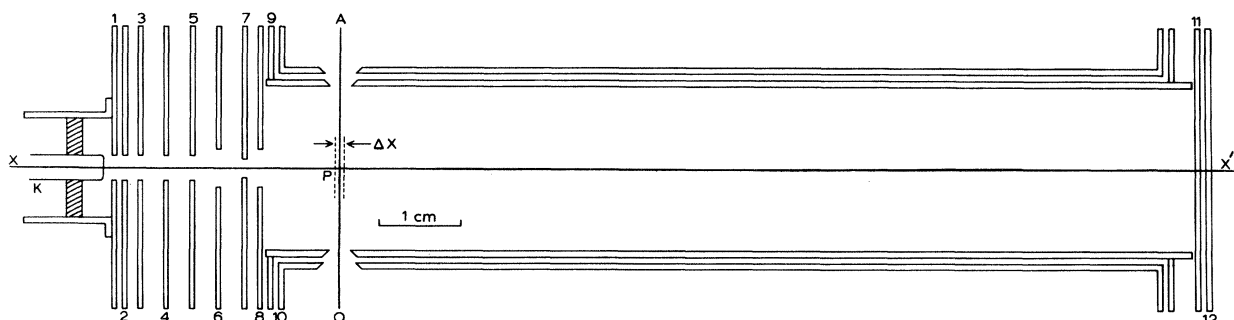


FIG. 2. Scale drawing of section through the electron gun, containing the electron-gun axis XX' and the orthogonal axis OA of the external optics. K is an indirectly heated cathode.

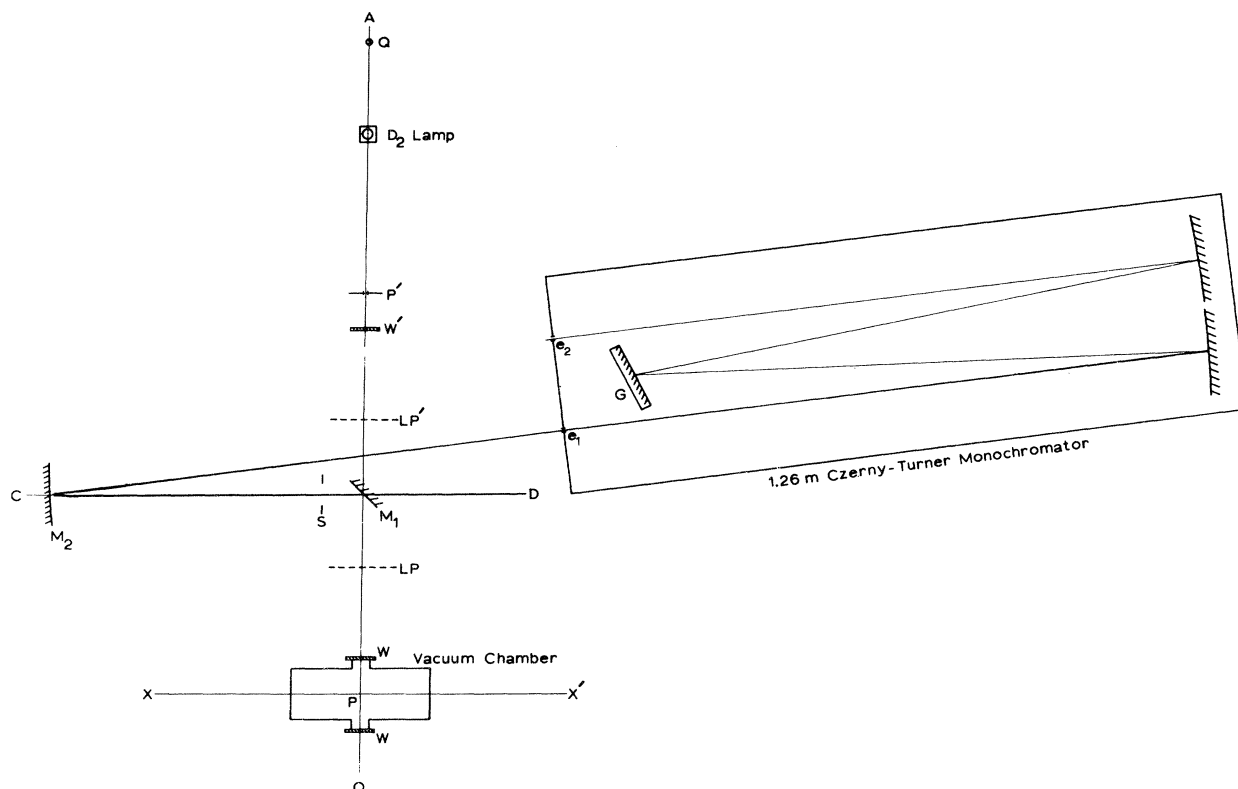


FIG. 3. Schematic diagram of the optical system used to measure the absolute intensity and polarization of light emitted by the electron-beam excited gas. Relative spacing of all optical components is shown to scale.

ty of point P , when the cup bottom (element 11) was biased positive with respect to the cylinder 9, in a test for secondary and reflected electrons from the cup bottom. Elements 5, 6, and 7 were included as a saddle field lens to allow better collimation of the beam in the region about point P at low energies. Its action was not found to be helpful at low energies, however, and also there was evidence that its field penetrated into the interior of the Faraday cup. Thus this lens was *not* used in any of the work reported here, and all three elements 5, 6, and 7 were held at ground potential. From study of the spatial distribution of intensity (see Sec. IV), the beam collimation in the region about point P was judged to be satisfactory. The nickel-tungsten alloy, oxide-coated cathode K was indirectly heated by a 4 W, double-helix-type heater. The coaxial cylinder labeled 10 and the plate labeled 12 were included to prevent the Faraday cup from collecting current on its outer surfaces, since radiation from the interior is not related to this current. Typically, $(I_{10} + I_{12}) < 0.01(I_8 + I_9 + I_{11})$. The electron-gun metal parts are type-304 stainless steel. The numbered plates in Fig. 2, as well as the insulating alumina spacers and support rods (not shown) are commercially supplied standard parts.

The optical detection system was calibrated from its response to the continuum radiation from a 40-W deuterium lamp (Optronics Laboratories Model UV-40) of known spectral irradiance. The first surface plane mirror M_1 was rotated 90° clockwise from the orientation shown in Fig.

3. The image of e_1 , formed by M_2 , then coincides with the position P' , obtained by reflecting P in the line CD . The deuterium lamp is positioned along OA , at a distance l_0 from the position P' , where $l_0 (= 30 \text{ cm})$ is the distance for which the lamp's calibration applies. The 3.2-mm-thick, uv grade fused silica plate W' is to compensate for the vacuum chamber window W , also 3.2-mm-thick uv grade fused silica. Light traveling from the lamp and through the entrance slit will undergo the same reflection and transmission losses as the light coming from the electron-beam-excited gas. When using the deuterium lamp, the vertical extent (perpendicular to plane of Fig. 3) of the receiver area is defined by a horizontal slit (not shown in Fig. 3) of width w (ordinarily $w = 0.397 \pm 0.002 \text{ mm}$), placed $\sim 0.25 \text{ mm}$ in front of the monochromator entrance slit.¹⁰ This horizontal slit could be precisely translated up and down (perpendicular to plane of Fig. 3), and allowed us to study the radial extent of the emitting region in the gas. Based upon the available lifetime data of 14 nsec for the $D^3\Sigma_u^+$ state¹¹ and 0.9 nsec for the $c_4'(0)^1\Sigma_u^+$ state,¹² and assuming a 300-K Boltzmann velocity distribution for the N_2 gas molecules ($\bar{v} = 4.2 \times 10^4 \text{ cm/s}$), the average distances traveled by a $D^3\Sigma_u^+$ and a $c_4'(0)^1\Sigma_u^+$ state molecule before decay are 0.006 and 0.0004 mm, respectively. The consequent minute expansion of the excited-molecule spatial distribution into regions outside the electron flux distribution will have a completely negligible effect upon the shape and absolute magnitude of the cross-section data reported here.

The local target gas density ρ_g in the region about P (Fig. 2) was determined using a Baratron¹³ capacitance manometer, although the procedure was complicated by what we will call the *local gas-heating effect*: The hot cathode K radiatively heats the surrounding electron-gun parts and consequently also heats the gas in the vicinity of these parts. In an earlier experiment, using an electron gun almost identical to the one in the present experiment, we measured with thermocouples the temperature rise ΔT (K) above room temperature, at several locations on the electron gun. In this earlier experiment, the electron source was a 12-mm-long V -shaped filament of 0.076-mm-diameter tungsten operated at a power of 3–5 W, and a temperature of ~ 1600 –2000 K. The temperature rise of the cylinder and plate (labeled 1 in Fig. 2) surrounding the filament was $\Delta T_1 > 100$ K, and the temperature rise ΔT_8 at the edge of the hole in the plate labeled 8, just preceding the Faraday cup, ranged from 20 to 30 K, depending upon heater power. In the present experiment, the cathode heater is operated at a power of 4 ± 0.2 W, and we therefore expect temperature rises in the electron gun to be comparable to those in the earlier experiment using the V -shaped filament. To quantitatively determine the effect of this heating upon the local gas density our procedure was to monitor, as a function of time, the signal R_c , developed from the very intense N_2 second positive (0,0) band. With the electron gun initially at room temperature, we turned on the cathode heater at a constant power of 3.9 W (normal heater power) and began measuring the second positive (0,0) band signal R_c every five minutes. Between measurements the beam was shut off. The electron-gun voltages and electron-beam current were held constant during this test. The observation is that the signal R_c decreased with elapsed time and reached an approximately time-independent value after about six hours [see Fig. 4(a)]. During this test, the gas pressure indicated by the capacitance manometer did not change significantly from its initial value of $p_0 = 4$ mTorr, set at the beginning of the test. From this observation we conclude that as the electron gun warms up from room temperature to its equilibrium temperature distribution, the local gas density ρ_g in the region about point P decreases. A second test, which confirmed the result of this first test but also gave more information, was the following. With the electron gun initially at room temperature, we turned on the cathode heater at the same constant power as in the first test and made a continuous recording of the second positive (0,0) band signal as a function of the analog signal V_m from the capacitance manometer. The gas was admitted through a leak valve and about five minutes were required for the pressure in the chamber to go from 0 to 4 mTorr. As before, the electron-gun voltages and currents were held fixed during this test as the signal R_c was recorded on the Y channel, while the analog voltage V_m from the manometer drove the X axis of the recorder. Then, after a 6-h interval, during which the cathode heater was left on, the plot of R_c vs V_m was repeated, giving the result that the plot of R_c vs V_m had precisely the same functional dependence on V_m as the curve obtained with the electron gun at room temperature, but was everywhere reduced by a factor of 0.875. This result is shown

in Fig. 4(b), where we have plotted the signal R_c , obtained with the electron gun at its equilibrium temperature distribution with the cathode heater on, against the signal R_c obtained with the electron gun at room temperature, $24 \pm 1^\circ\text{C}$. From these two tests we conclude that the percent reduction in local gas density caused by the hot cathode is *independent* of the pressure over the range studied (0–4 mTorr). The effect of thermal transpiration was also investigated¹⁴ and found to have negligible ($< 0.5\%$) effect on the gas-pressure measurement. Thus in this work the target gas density ρ_g in the region about point P (Fig. 2) was determined from

$$\rho_g = 0.875p/kT_r, \quad (5)$$

where k is Boltzmann's constant, p is the collision chamber gas pressure, and T_r is room temperature.

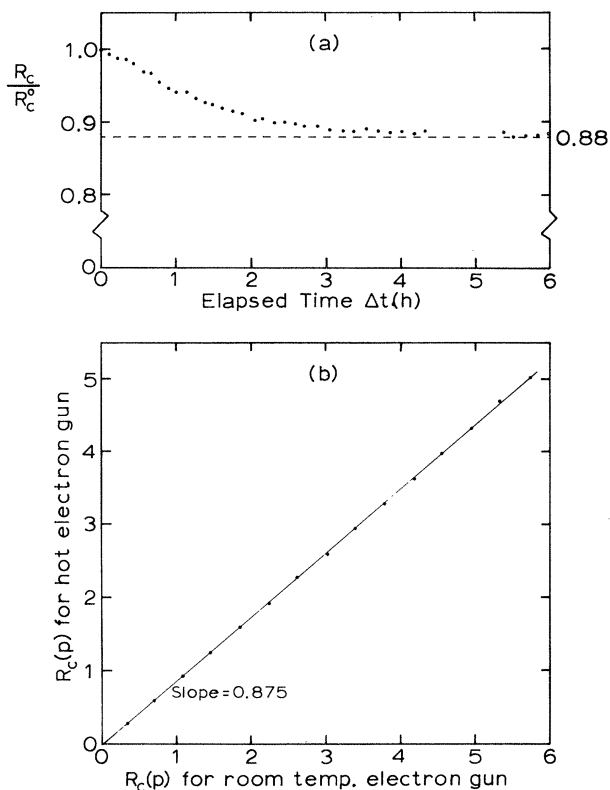


FIG. 4. (a) Signal developed from N_2 second positive (0,0) band vs elapsed time Δt following turn-on of the cathode heater at normal power of 3.9 W. Manometer pressure $p = 4$ mTorr, electron-beam energy $E = 20$ eV, and electron-beam current $I = 100 \mu\text{A}$. At $\Delta t = 0$, electron gun is at room temperature (297 ± 1 K) and signal is R_c^0 . (b) Comparison of signal developed from N_2 second positive (0,0) band with electron gun at room temperature, and with electron gun at equilibrium temperature distribution corresponding to a heater power of 3.9 W. Electron energy $E = 14.3$ eV and electron-beam current $I = 5.3 \mu\text{A}$. Pressure was varied over range $0 \leq p \leq 3.75$ mTorr. The same arbitrary unit has been used for both ordinate and abscissa. The least-squares-fitted straight line shown here has slope equal to 0.875.

TABLE I. Maximum optical-emission cross sections and branching ratios as determined in this work for bands of the $D^3\Sigma_u^+(v'=0) \rightarrow B^3\Pi_g(v'')$ system of N_2 , along with our error estimates for these experimental values.

N_2 $D^3\Sigma_u^+ \rightarrow B^3\Pi_g$ ($0, v''$)	Shortest-wavelength band head ^a (Å)	Maximum optical-emission cross section ^b $Q_{opt}(0, v'')$ (10^{-20} cm ²)	Estimated error ^c in cross section (%)	Branching ratio $\Gamma_{0v''}$	Estimated error ^c in branching ratio (%)
(0,0)	2256.0	2.26	11	0.178	7
(0,1)	2346.4	3.57	8	0.281	6
(0,2)	2442.8	3.15 ^d	10	0.248 ^d	6
(0,3)	2545.3	1.90 ^e	11	0.149 ^e	7
(0,4)	2654.5	1.05	10	0.083	6
(0,5)	2771.4	0.56	10	0.044	6
(0,6)	2896.6	0.22	10	0.017	6

^aWavelength data from Ref. 15, p. 230.

^bMaximum cross section occurred at 14.1 ± 0.3 eV. See Fig. 7. The (0,1) band cross section was determined directly from knowledge of all quantities in Eq. (7). The other six cross sections for $v'' \neq 1$ were determined from $Q_{opt}(0, v'') = (\Gamma_{0v''}/\Gamma_{00})Q_{opt}(0, 0)$, where the Γ 's are the separately determined branching ratios. See column 5.

^cThis figure obtained by adding in quadrature the estimated errors from all sources, including 0.2–0.7% error due to variation in detection system sensitivity over the wavelength span of a band.

^dThe (0,2) band was partially overlapped by another molecular band with threshold at ≈ 14.2 eV and maximum at ≈ 14.9 eV. This band could not be identified with any molecular band given in Ref. 15. Since our cross-section and branching-ratio measurements were made at ≈ 14.1 eV, which is just below threshold for this unidentified band, this difficulty with the (0,2) band measurement was avoided.

^eCorrection was made for partial overlap of the (0,3) band by the Herman-Kaplan $E^3\Sigma_g^+ \rightarrow A^3\Sigma_u^+(0,5)$ band.

III. PROCEDURES AND RESULTS FOR $D^3\Sigma_u^+(v=0)$

Because our results differ from other experimental work, we describe fully our experimental procedures, along with our results. We have observed all seven of the fourth positive bands reported in the literature: $D(v'=0) \rightarrow B(v''=0,1,2,3,4,5,6)$.¹⁵ See Fig. 1(a) and Table I. After examination of each of them with regard to overlapping by bands or lines of other systems, and also signal-to-noise ratio, we found the (0,1) band to be the most favorable for experimental investigation of the dependence of the $D^3\Sigma_u^+(v=0)$ emission on target gas pressure, electron-beam current, incident electron energy, and also for the determination of the polarization \mathcal{P} of the $D \rightarrow B$ radiation. Our procedures for this investigation are illustrated by Fig. 5, which is a spectral scan of the (0,1) band at a resolution of 1 Å.

With the monochromator passband [usually triangular, 4 Å full width at half maximum (FWHM) centered on, or very close to the shortest-wavelength head of the fourth positive (0,1) band (position *a* in Fig. 5), we studied the pressure dependence of the photomultiplier signal developed, while all other parameters were held fixed. This measurement was made many times, at a variety of electron-beam energies and currents. The signal developed at position *a* has an additive background contribution caused by light which reaches the PMT photocathode after being scattered within the monochromator. With the passband shifted to position *b* in Fig. 5, we studied the background signal and found it to be proportional to pressure and to have an energy dependence shown by the inset curve *b* of Fig. 5. Because of its very weak dependence on grating rotation angle, the background signal at position *a*

is practically the same as that measured at position *b*. In Fig. 6 we show some of our results for the pressure dependence of the fourth positive (0,1) band signal, where we have plotted *total* signal at position *a*, i.e., fourth positive (0,1) band signal plus the background signal. Since the background was found to be proportional to pressure, then deviation of the total signal from linearity with the pressure reveals a nonlinear behavior of the fourth positive (0,1) band signal. In Fig. 6, the data for the curves at each

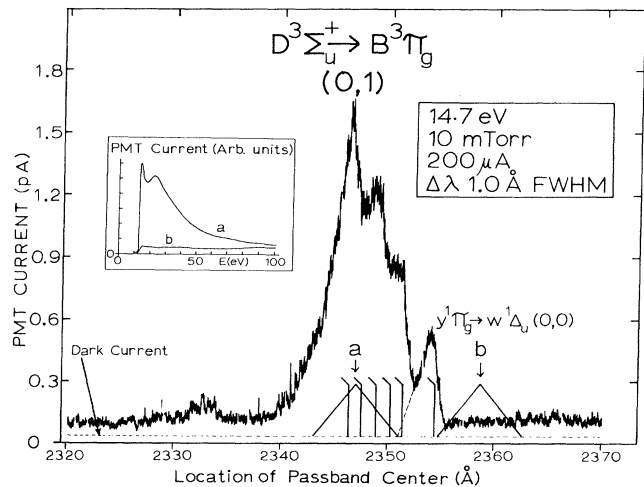


FIG. 5. Signal developed from spectral scan of the N_2 $D^3\Sigma_u^+ \rightarrow B^3\Pi_g$ fourth positive system (0,1) band, using triangular spectral passband of 1 Å FWHM. Flags on band head markers indicate the violet-degraded shading of the bands. The triangular passband shown is 4 Å FWHM.

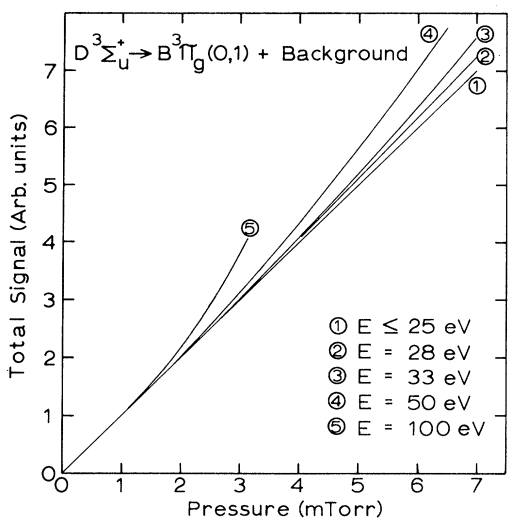


FIG. 6. Illustration of nonlinearity with pressure in signal developed from the $N_2 D^3\Sigma_u^+ \rightarrow B^3\Pi_g(0,1)$ band. Plotted here is total signal [i.e., $D \rightarrow B(0,1)$ band signal + background] obtained with a triangular passband of $\Delta\lambda = 4 \text{ \AA}$ FWHM centered on or very close to position a of Fig. 5. The background, which was found to be proportional to pressure over the pressure range of Fig. 6, makes up about 8, 8, 12, 21, and 74% of the total signal at energies of 25, 28, 33, 50, and 100 eV, respectively. To facilitate comparison, each curve has been scaled as necessary to make all the curves have the same slope in the low-pressure region where the total signal is proportional to pressure. The data generally lie within a few percent of these least-squares-fitted curves.

energy have been scaled as necessary to make them all agree in slope in the low-pressure region where total signal is proportional to the pressure. This is done only to facilitate comparison of the data. To be sure that this non-linear behavior was not caused by some unnoticed foreign signal, we repeated some of the signal-versus-pressure measurements using the fourth positive system (0,2) band (see Table I) and again found the same pressure dependence as with the (0,1) band. Our results for the dependence of the fourth positive intensity on target gas pressure (Fig. 6) are qualitatively characterized by a deviation from linearity which begins to occur at lower and lower pressures as we raise the electron energy. For example, the signal begins to show deviation from linearity with pressure, above pressures of approximately 3.5, 3, 2, and 1.25 mTorr at incident electron energies of 28, 33, 50, and 100 eV, respectively.

Using a triangular passband of 4 \AA FWHM at position a (Fig. 5), we studied the dependence of the fourth positive (0,1) band intensity on electron-beam current I , over the range $I \leq 300 \mu\text{A}$, where $I = I_8 + I_9 + I_{11}$ is the sum of the currents collected at the electron-gun elements labeled 8, 9, and 11 in Fig. 2. Just as in the case of the intensity-versus-pressure data, we found an energy-dependent deviation from a linear dependence of the intensity on the current. However, in this case the deviation was in the

opposite sense to that observed in the intensity-versus-pressure data, i.e., the intensity increased at a rate which was *less* than in direct proportion to the current. Our results for the current dependence of the (0,1) band intensity are not as simply characterized as those for the pressure dependence (Fig. 6). For the purposes of this experiment though, we can say that for pressure $p < 3$ mTorr, the $D \rightarrow B(0,1)$ band signal was directly proportional to the current for $I < 100 \mu\text{A}$, independently of the electron energy. All our measurements of the energy dependence of the $D \rightarrow B$ optical emission, as well as the absolute magnitude of the optical-emission cross sections, have been made at sufficiently low pressure and current that the intensity is directly proportional to the pressure and current.

We studied the dependence of the $D \rightarrow B$ emission on the energy of the incident electrons by recording the (0,1) band signal developed with a 4-\AA FWHM passband at position a in Fig. 5, as a function of the energy, all other parameters held constant. However, since the background has an energy dependence which is distinctly different from that of the fourth positive emission, we also determined the energy dependence of the background signal at position b (Fig. 5). This is shown by the inset curve (b) of Fig. 5. The difference of the signals obtained at positions a and b thus more accurately represents the energy dependence of the $D^3\Sigma_u^+(v=0)$ emission. Higher-resolution scans ($\Delta\lambda < 1 \text{ \AA}$) of the $D \rightarrow B(0,1)$ band showed that with a triangular passband of FWHM $\leq 4 \text{ \AA}$ and centered on position a , the contribution of the (0,0) band of the $y^1\Pi_g \rightarrow w^1\Delta_u$ Kaplan second band system¹⁵ (see Fig. 5) is negligible in comparison with the $D \rightarrow B(0,1)$ band. Using a much smaller passband ($\Delta\lambda = 1 \text{ \AA}$ FWHM) at a position 1.2 \AA to the right of position a in Fig. 5, we repeated the measurements of the energy dependence of the $D \rightarrow B(0,1)$ band signal from threshold to 60 eV; the result was indistinguishable from that obtained using the 4-\AA passband at position a , thus strongly supporting the implicit assumption we have made in this work, that the intensity of each component of the band has the same dependence on incident electron energy. Our background-corrected results obtained in this way for the energy dependence of the fourth positive (0,1) band intensity are shown in Fig. 7 in a linear-linear plot from threshold to 60 eV. These results are also shown in Fig. 8 in a log-log plot from threshold to 100 eV. In determining the energy dependence of the (0,1) band intensity (Figs. 7 and 8), our choice of target gas pressure was guided by the signal-versus-pressure data of Fig. 6: For electron energy $E \leq 28$ eV, pressures of 2 and 3 mTorr were used. For $E > 28$ eV, pressures of 0.5 and 1 mTorr were used. There was no obvious difference between the energy dependence at 0.5 and 1 mTorr, nor was there any difference between the energy dependence at 2 and 3 mTorr for $E \leq 28$ eV. Above ~ 65 eV, the log-log plotted data of Fig. 8 are fairly well described by a straight line of slope -3 , indicating an asymptotic E^{-3} energy dependence for the optical-emission cross section. This asymptotic E^{-3} energy dependence is also expected on theoretical grounds,¹⁶ for the electron collision-induced, spin-forbidden transition $X^1\Sigma_g^+ \rightarrow D^3\Sigma_u^+$.

Although we used the $D \rightarrow B(0,1)$ band for most of our studies, we did verify, by obtaining relative optical-

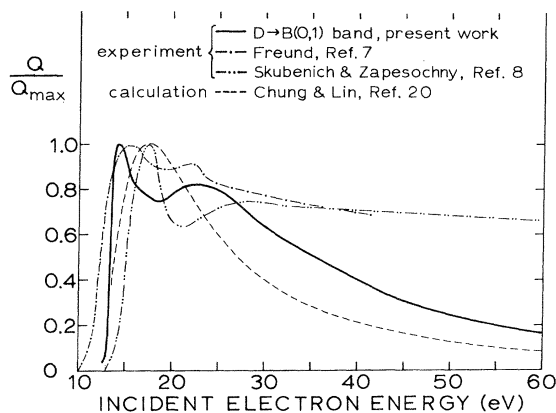


FIG. 7. Comparison of the energy dependence of the $D^3\Sigma_u^+ \rightarrow B^3\Pi_g(0,1)$ band as determined in this work with the results of other experiments, and with the cross-section calculation of Ref. 20 for the direct electron-impact excitation of the $N_2 D^3\Sigma_u^+$ state. The results of the present work (represented by the solid curve) have been corrected for the energy-dependent background. We believe that relative to the maximum at 14 eV, the shape of the curve (solid line) representing the present results is correct to within 5% for energies $14 \leq E \leq 60$ eV. For each curve, the data have been normalized to their maximum.

emission excitation functions for all the fourth positive bands, that each of the bands of the $D \rightarrow B(0, v'')$ sequence (Table I) exhibited the double maxima shown in the (0,1) band data of Fig. 7.

Based upon the dependence on accelerating voltage in the vicinity of threshold (11.03 eV) for the very intense N_2 second positive $C^3\Pi_u \rightarrow B^3\Pi_g(0,0)$ band emission, we estimate that, for the work reported in this paper, the full width at base (FWAB) of the electron energy distribution was < 0.5 eV. The energy scales (eV) used in Figs. 7 and 8 were generated by shifting the zero of the uniform voltage scales used in obtaining the data, so that the threshold occurs at 12.84 V as predicted from spectroscopic data.¹⁵ For the pressures and currents used in this work, the shift was -1.9 ± 0.2 V and was stable over a one year period of electron-gun operation. This difference between the incident electron energy E (eV) and the accelerating voltage V_{kg} applied between cathode and ground results from a combination of effects: (a) penetration of externally generated electric fields into the interior of the Faraday cup; (b) electric field generation within the Faraday cup by the charge distribution of the electron beam itself; (c) a small contact potential difference of at most ~ 0.2 V, caused by dissimilar metal junctions in the external cathode-ground circuit; and (d) charged dielectric surface layers around the edges of the apertures in the electron-gun elements, presumably caused by electron bombardment of adsorbed layers of diffusion pump fluid. We found this last item (d) to be quite troublesome in an earlier experimental apparatus in which silicone diffusion pump fluid was used, even though a liquid-nitrogen-cooled cold trap was used between the pump and the collision chamber, just as in the present work. In this earlier apparatus, the offset ($V_{kg} - E$) would often reach a value of 10 V or more over a period of 20–40 h of electron-gun operation, and this

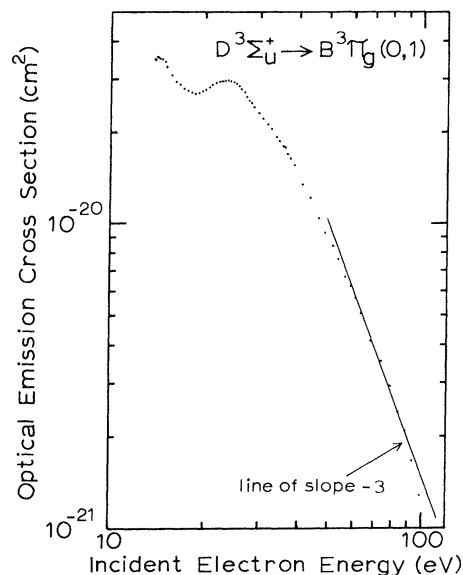


FIG. 8. Log-log plot of the $D^3\Sigma_u^+ \rightarrow B^3\Pi_g(0,1)$ band absolute optical-emission cross section determined in this work, as a function of the incident electron energy E . These same data are represented by the smooth solid curve in Fig. 7. Above ~ 65 eV, the energy dependence of these data is fairly well described by the form E^{-3} .

necessitated frequent cleaning of the electron-gun elements. In the present work, an all-hydrocarbon type of diffusion pump fluid was used, and the diffusion pump was used only long enough (10–15 sec) to pump out a target gas sample. The rest of the time, the collision chamber was pumped by an ion pump. We attribute this long term stability of the offset to the use of the all-hydrocarbon pump fluid and to minimal use of the diffusion pump.

Another significant experimental problem common to all the work reported in this paper, and distinct from the local gas-heating effect already discussed, is that of non-constant target gas pressure. We found that the target gas pressure decreases at a rate proportional to the electron-beam current. The rate of the decrease of pressure, at constant electron-beam current I , also is proportional to the pressure p and depends on the incident electron energy E , i.e., $\dot{p} \simeq -k(E)pI$, where $k(E)$ is an energy-dependent factor. This effect, which has not been reported in electron-impact excitation studies of monatomic gases, is presumably related to dissociative electron-impact excitation of the N_2 . We observed that the rate of decrease \dot{p} of the pressure was largest for incident electron energies in the vicinity of 90 eV, where the cross section for dissociative electron-impact excitation of N_2 also is maximum.⁵ Since the pressure decreases, then apparently the total number of gas particles also decreases, a result which seems puzzling because the dissociation of one N_2 molecule will yield two atomic fragments ($N + N$ or $N + N^+$). One possible explanation is that the atomic fragments are adsorbed by the surfaces of the vacuum chamber and electron gun. Assuming the atomic fragments from each N_2 dissociation are permanently adsorbed and using the max-

imum cross section of $2 \times 10^{-16} \text{ cm}^2$ reported by Ref. 5 for dissociative electron-impact excitation of N_2 , a simple calculation of the expected rate constant $k(E)$ yields a maximum value of $0.009 \text{ h}^{-1} \mu\text{A}^{-1}$ for the chamber volume and electron-gun geometry of the present work. The fact that the rates $k(E)$ we obtain from our data are generally a factor of 40–70 smaller than this calculated maximum rate could indicate that adsorption of the atomic fragments does occur, but that an adsorbed atom remains on the surface only a finite length of time. Depending upon the energies and the time-integrated currents used in obtaining a particular set of data, we observed pressure decreases which were as large as 9% of the initial pressure set in the vacuum chamber. Since our $D \rightarrow B$ data were obtained at pressures for which signal is proportional to pressure, then our correction procedure was simple multiplication of the light signal R_c by the factor (p_0/p) where p is the instantaneous pressure corresponding to R_c and p_0 is the reference pressure, which was generally chosen to be the initial pressure. In obtaining the continuous plots of signal versus pressure (see Fig. 6), the time intervals required were sufficiently short (≤ 12 minutes) that there was no significant distortion introduced by this effect. For the signal-versus-current and signal-versus-energy data, which generally were obtained point by point with total beam-on time intervals as long as 2 h, the above correction was applied. Also, the pressure value that we associated with the integrated intensity of a band was the pressure value which occurred at the position of the centroid wavelength in the spectral scan of the band.

Measurements of the percent polarization \mathcal{P} (%) of the fourth positive (0,1) band radiation were made using a dichroic polymer film uv linear polarizer (Oriental Corporation Model 2732) where

$$\mathcal{P} \equiv 100 \% \left[\frac{\mathcal{I}_{\parallel} - \mathcal{I}_{\perp}}{\mathcal{I}_{\parallel} + \mathcal{I}_{\perp}} \right] \quad (6)$$

and $\mathcal{I}_{\parallel}, \mathcal{I}_{\perp}$ are the emission intensities per unit solid angle in a direction perpendicular to the electron-beam direction, for radiation with electric field vector parallel and perpendicular, respectively, to the electron-beam direction. The polarizer was placed at locations LP' and LP (see Fig. 3) in order that the particular polarization component (parallel or perpendicular) could be selected before it was sent through the optical system. With the polarizer at position LP' of Fig. 3, we determined the ratio of the detection system responses to the two polarizations, using the deuterium lamp as an unpolarized source. A repeat of this ratio measurement, using a coiled tungsten helix in quartz envelope lamp at position Q of Fig. 3, gave the same result within 0.5%. With the linear polarizer at position LP , we determined the ratio of signals developed from the two background-corrected components of the $D \rightarrow B$ (0,1) band radiation. In extracting polarization values from our measurements we took into account the fact that the polarizer is an imperfect device, i.e., $\kappa_2/\kappa_1 \simeq 0.03 \neq 0$ where κ_2 and κ_1 are the intensity transmittance factors of the polarizer for light polarized perpendicular and parallel, respectively, to the direction for maximum transmission of the polarizer. Our polarization

measurements were made at a pressure of 4 mTorr over the energy range 13–23 eV and 2 mTorr for energies 23–31 eV. The individual polarization measurements were scattered within a range $-5\% \leq \mathcal{P} \leq +5\%$. The scatter appeared random however, and the average of the polarization measurements was very close to zero (-0.1%). This indicates that the $D \rightarrow B$ radiation is *unpolarized* and consequently, the energy dependence of the optical-emission signal, as measured in this experiment, using only a very small fraction ($\Omega_c/4\pi \simeq 0.0006$) of the radiation, is representative of the energy dependence of the angle-integrated optical emission per unit beam length.

The $D \rightarrow B$ (0,1) band relative optical-emission data given in Fig. 7 were converted to absolute values (Fig. 8) by measuring the absolute magnitude of the (0,1) band optical-emission cross section at 14.1 eV, where the cross section reaches its principal maximum. A gas pressure of 3.5 mTorr and beam current of $60 \mu\text{A}$ were used for these measurements. Figure 5 illustrates our procedure for determining the absolute magnitude of the $D \rightarrow B$ (0,1) band cross section. We measured the area \mathcal{R}_c under the curve obtained from the spectral scan of the (0,1) band, accounting as necessary for overlapping by the Kaplan second $y^1\Pi_g \rightarrow w^1\Delta_u$ (0,0) band, and using as baseline a straight line connecting the background signal levels on either side of the fourth positive band. Then, the passband was centered on the position corresponding to the centroid wavelength of the spectral scan of the band, and with plane mirror M_1 rotated 90° clockwise from the position shown in Fig. 3, we obtained the response R_s developed from the deuterium lamp. For both the spectral scan of the band and the response R_s developed from the deuterium lamp, the monochromator slit widths were set to yield a triangular passband of 1.5 \AA FWHM at $\lambda = 2350 \text{ \AA}$. From these data, the absolute optical-emission cross section for the band was calculated using expression (7):

$$Q_{\text{opt}}(v', v'') = \left[\frac{4\pi w \mathcal{L} \mathcal{R}_c}{(I/e)\rho_g \Omega_c M R_s} \right] Z(\mathcal{P}), \quad (7)$$

where \mathcal{L} is the spectral irradiance of the deuterium lamp, M is the lateral magnification with which spherical mirror M_2 images the electron-gun axis XX' onto the entrance slit ($M = 1.000 \pm 0.002$), w is the width of the horizontal slit placed next to the entrance slit and determines the vertical extent of the receiver area in the absolute calibration procedure ($w = 0.397 \pm 0.002 \text{ mm}$), and Z is a correction function to account for the case in which the molecular band radiation has linear polarization \mathcal{P} (%), with $Z = 1$ when $\mathcal{P} = 0$. The other quantities have already been defined in the text. From this measured maximum absolute (0,1) band cross section and the measured branching ratios $\Gamma_{0v''}$, we determined the maximum absolute magnitude of the other six cross sections of the $D \rightarrow B$ (0, v'') sequence.

The branching ratios $\Gamma_{0v''} \equiv Q_{\text{opt}}(0, v'') / \sum_{v'''} Q_{\text{opt}}(0, v''')$ for the bands of the $D \rightarrow B$ (0, v'') sequence were also determined at 14.1 eV, but at larger pressure and current of 7 mTorr and $150 \mu\text{A}$, in order to increase the precision of the branching-ratio determination. Although the signals were then slightly nonlinear with

current, the spectral scans of all the bands were carried out under the same conditions so that the cross-section ratios determined from these data were not affected by the nonlinearity with current, since they all correspond to a common upper level.

Our results for the maximum values of the optical-emission cross sections for the seven bands of the $D^3\Sigma_u^+ \rightarrow B^3\Pi_g$ fourth positive band system and the corresponding branching ratios are shown in Table I, along with our error estimates for these values.

IV. PROCEDURES AND RESULTS FOR $c'_4 \ ^1\Sigma_u^+(v=0)$

The previous work of Refs. 4, 5, and 6 was carried out using bands of the $c'_4 \ ^1\Sigma_u^+ \rightarrow X \ ^1\Sigma_g^+$ system,¹⁵ which occurs in the extreme-uv spectral region ($\lambda < 1100 \text{ \AA}$). In the present work, we have investigated excitation of the $c'_4(v=0)$ state by studying the electron-impact production of the $(0, v'')$ bands of the $c'_4 \rightarrow a \ ^1\Pi_g$ band system,¹⁵ which occur in the near-uv spectral region 2800–3700 \AA [see Fig. 1(b)]. In particular, we used the $(0,0)$ and $(0,4)$ bands to study the dependence of the $c'_4(v=0) \rightarrow a$ signal on electron-beam current, target gas pressure, and incident electron energy. Other bands of the $c'_4 \rightarrow a(v', v'')$ system for $v'=1, 2, 3,$ and 4 were tentatively identified in surveys of the near-uv spectrum of N_2 . These other bands were much less intense than the bands of the $c'_4 \rightarrow a(0, v'')$ sequence, and we did not attempt to study them. The procedures we followed, which were generally the same as those already described in Sec. III, are illustrated by Fig. 9, which is a spectral scan at a resolution of 0.5 \AA of the region containing the $c'_4 \rightarrow a(0,0)$ band.

With a 4.6 \AA FWHM trapezoidal passband centered on position a (Fig. 9), we studied the total signal [i.e., $c'_4 \rightarrow a(0,0) + \text{background}$] developed as a function of the electron-beam current I for $0 \leq I \leq 200 \text{ \mu A}$. Although

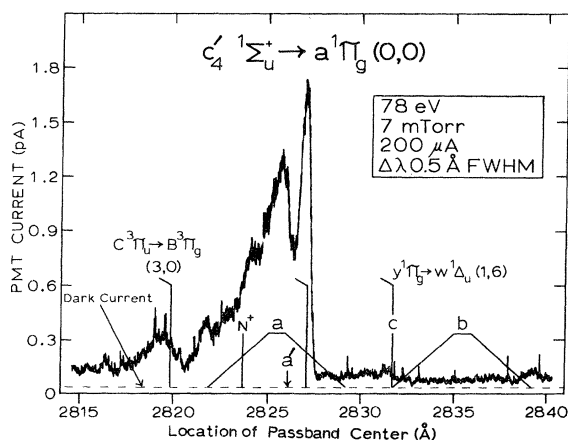


FIG. 9. Signal developed from spectral scan of the N_2 $c'_4 \ ^1\Sigma_u^+ \rightarrow a \ ^1\Pi_g(0,0)$ band, using a triangular spectral passband of 0.5 \AA FWHM. Figure 9 is used only to illustrate the procedures followed in this work. At the N_2 pressure of 7 mTorr used in Fig. 9 the $c'_4 \rightarrow a$ signal is definitely not proportional to pressure. See $c'_4 \rightarrow a$ signal-vs-pressure curves of Fig. 10. Flags on the band head markers indicate the violet-degraded shading of the bands. The trapezoidal passband shown is 4.6 \AA FWHM.

with this passband the $N^+ \ 2s^2 2p \ 4p \ ^1P \rightarrow 2s \ 2p^3 \ ^1P$ line at 2823.635 \AA is transmitted with about 70% relative efficiency, it makes at most a 3–4% contribution to the total signal. Furthermore, in a separate investigation we found the N^+ line signal to be proportional to the current for the pressures and currents used in the present work. Thus it does not introduce any nonlinearity in the dependence of the total signal on current. For energies in the range 25–60 eV, the total signal developed at position a did exhibit some deviation from a linear dependence on current for currents $I > 100 \text{ \mu A}$: The signal began to increase at a rate greater than direct proportion to the current. (This is opposite to the deviation from linearity we observed in the $D \rightarrow B$ signal-versus-current data. See Sec. III.) The deviation of the total signal from a linear dependence on current was largest at an energy of $\sim 30 \text{ eV}$, with the signal at $I=200 \text{ \mu A}$ and $p=5 \text{ mTorr}$ being about 16% larger than expected from a linear extrapolation of the lower-current data. However, for currents $I \leq 100 \text{ \mu A}$, the total signal was proportional to current, for energies $E \leq 100 \text{ eV}$, when the pressure was kept below 5 mTorr (the largest pressure used in the signal-versus-current studies). We have assumed this to mean that the $c'_4 \rightarrow a$ signal itself is also proportional to current I for $I \leq 100 \text{ \mu A}$ and pressures $p \leq 5 \text{ mTorr}$. Also, we found that at $p=1 \text{ mTorr}$ and $E=200 \text{ eV}$ the total signal is proportional to current I for currents $I \leq 200 \text{ \mu A}$. We mention this here because these are the conditions of pressure, energy, and current under which our $c'_4 \rightarrow a$ absolute

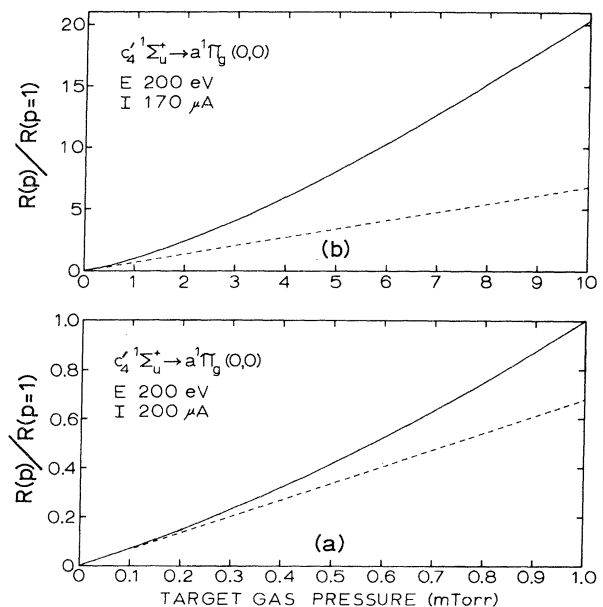


FIG. 10. Dependence of the background-corrected $c'_4 \rightarrow a(0,0)$ band signal $R(p)$ on target gas pressure p (mTorr). Curve in (a) is the least-squares-fitted quadratic polynomial representation of the data, scaled to have value 1 at $p=1 \text{ mTorr}$. Dashed straight line is the linear part of the quadratic polynomial fit. It has value 0.679 at $p=1 \text{ mTorr}$. Curve shown in (b) is the least-squares-fitted cubic polynomial representation of the data over the pressure range $0-10 \text{ mTorr}$, also scaled to have value 1 at $p=1 \text{ mTorr}$. Dashed straight line is the same line shown in (a).

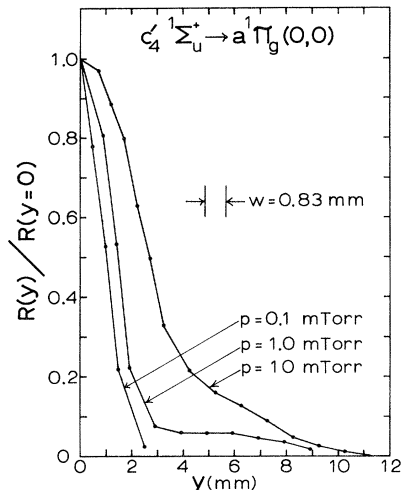


FIG. 11. Illustration of pressure effect on the spatial extent of the emitting region using as signal source the $c'_4 \rightarrow a$ (0,0) band at constant electron energy of 70 eV and beam current of 200 μA . $y(\text{mm}) = Y - Y_0$, where Y is the coordinate giving the location of the center of the vertically translatable slit of width $w = 0.83$ mm and Y_0 is the slit coordinate for which the signal $R(y)$ is a maximum. $R(y)$ is the total signal, i.e., $c'_4 \rightarrow a$ (0,0) + background.

optical-emission cross-section measurements were made.

For the pressure dependence of the $c'_4 \rightarrow a$ intensity we found a very marked deviation from a linear dependence on the pressure. This is illustrated by Fig. 10 in which we show the pressure dependence of the signal developed from the $c'_4 \rightarrow a$ (0,0) band. The data shown in Fig. 10 were obtained with a 2.4 \AA FWHM triangular passband centered on position a' , so as to just exclude any contribution from the N^+ line at 2823.635 \AA . See Fig. 9. These data have also been background-corrected by subtraction of the proportional-to-pressure background measured with the passband shifted to position b . The $c'_4 \rightarrow a$ (0,0) band signal begins to show significant deviation from a linear dependence on pressure for pressure $p > 0.1$ mTorr. In studies of electron-impact-produced emission from the $c'_4(v=0)$ state, Refs. 4, 5, and 6 also reported significant deviations from a linear dependence on pressure. For the $c'_4 \rightarrow X(v',0)$ transitions Ref. 5 reported a deviation from linearity with pressure which was in the opposite sense to what we show in Fig. 10 and for the $c'_4 \rightarrow X(0,1)$ band, the intensity was enhanced with respect to a linear dependence, similar to what we show in Fig. 10. Reference 6, which work was done using crossed molecule and electron beams, indicated that significant nonlinearity in the $c'_4 \rightarrow X(0,0)$ signal occurred for background pressures > 0.01 mTorr and in the $c'_4 \rightarrow X(0,1)$ signal for background pressure > 0.1 mTorr. The signal-versus-pressure data of Ref. 4 for the $c'_4 \rightarrow X(0,1)$ band was qualitatively similar to what we show in Fig. 10. As pointed out by these investigators, this nonlinear pressure dependence for the intensity of emission from the c'_4 state is caused by absorption of $c'_4 \rightarrow X(v',0)$ photons. See Fig. 1(b). $c'_4 \rightarrow X(v',v'')$ photons for $v'' > 0$ can also be absorbed but this is much less likely because the population of $X^1\Sigma_g^+(v'' > 0)$ molecules is very small compared with the population of

$X^1\Sigma_g^+(v=0)$ molecules. Each time a ground-state molecule $X^1\Sigma_g^+(v''=0)$ is raised to the $c'_4\ ^1\Sigma_u^+$ state by absorption of a $c'_4 \rightarrow X(v',0)$ photon, the excited molecule c'_4 has a probability of decaying to the $a^1\Pi_g$ state or some other vibrational level v'' ($v'' > 0$) of $X^1\Sigma_g^+$. This absorption and decay process effectively enhances the emission rate per unit length of the beam for the $c'_4 \rightarrow X(v'' > 0)$ and the $c'_4 \rightarrow a$ bands and reduces the emission rate for the $c'_4 \rightarrow X(0,0)$ band. Qualitatively we would expect that in our apparatus (see Fig. 2) as the target gas pressure is decreased, the mean distance \bar{l} traveled by a $c'_4 \rightarrow X(0,0)$ photon before absorption would increase and consequently the radial extent (perpendicular to XX') of the emitting region of the gas would increase. Experimentally, we found the opposite. The radial extent of the emitting region became smaller as we lowered the pressure. These results, which are shown in Fig. 11, were obtained by placing a slit of width $w = 0.83$ mm directly in front of the monochromator entrance slit and translating this slit up and down (perpendicular to plane of Fig. 3). The long direction of slit w is parallel to the plane of Fig. 3. In this way, we could sample the optical emission at different distances from the axis XX' of the electron gun. The three profiles shown in Fig. 11 were obtained at $E = 70$ eV and $I = 200$ μA . At pressures of 10, 1, and 0.1 mTorr the FWHM of the intensity profiles is 2.3, 1.3, and 0.9 times the diameter (2.4 mm) of the aperture in electron-gun element 7 (see Fig. 2). The aperture in element 7 is the smallest aperture in the electron gun. We observed very similar intensity profiles and pressure effects on this profile for the case of $D^3\Sigma_u^+ \rightarrow B^3\Pi_g$ and $C^3\Pi_u \rightarrow B^3\Pi_g$ emission which is unaffected by radiation trapping. We attribute the reduction in radius of the emitting region as the pressure is lowered, primarily to a reduction in the flux of electrons scattered out of the beam. Thus it appears that the mean free path \bar{l} for the extreme uv $c'_4 \rightarrow X(0,0)$ photons in the pressure range 0.1–10 mTorr, must be very short with respect to the observed change in radius of the emitting region over the same pressure range (i.e., $\bar{l} \ll 2$ mm), so that we simply do not see the associated expansion of the radius of the emitting region as we lower the pressure.

We investigated the energy dependence of the $c'_4 \rightarrow a$ signal using both the (0,0) and (0,4) bands. For the (0,0) band, the energy dependence of the optical emission was determined from the difference of the total signal [$c'_4 \rightarrow a$ (0,0) + background] measured at position a (Fig. 9) and the background signal measured at position b . This excitation-function measurement was made using pressures of 1, 4, and 5 mTorr and corresponding passband dimensions (centered on position a) of 2 \AA FWHM triangular, 4.6 \AA FWHM trapezoidal (shown in Fig. 9), and 2 \AA FWHM triangular, respectively. The resulting curves, each normalized to its maximum, were in very good agreement with each other, with the maximum difference between the curves being less than 5% at any energy from threshold to 200 eV. This indicates that the energy dependence of the $c'_4 \rightarrow a$ signal is practically pressure independent for $p < 5$ mTorr, even though the pressure dependence, at fixed energy, is decidedly nonlinear for $p > 0.1$ mTorr. See Fig. 10. As already mentioned, the N^+ line at 2823.635 \AA makes at most a 3–4% contribution to the

total signal measured at position a with the 4.6 Å FWHM trapezoidal passband. The fact that the curves obtained using $\Delta\lambda=4.6$ Å FWHM trapezoidal and $\Delta\lambda=2$ Å FWHM triangular (which will have no contribution from the N^+ line) agree so closely shows that the N^+ line contribution has no significant effect on the shape (energy dependence) of the data. Our measurements for the (0,0) band excitation function at $p=4$ mTorr, $I=100$ μ A using the 4.6 Å FWHM trapezoidal passband were extended to 440 eV, and the normalized results are shown in Fig. 12. These (0,0) band data include a correction for the contamination of the signal at passband position a by the violet-degraded $y^1\Pi_g \rightarrow w^1\Delta_u$ Kaplan second (1,6) band (see Fig. 9), as well as a correction for the continuum background (measured at position b). The first correction required an excitation function for the $y^1\Pi_g \rightarrow w^1\Delta_u$ (1,6) band, which we measured at position c . It also required knowledge of the spectral distribution of the $y \rightarrow w$ (1,6) band, which we approximated by the spectral distribution of the $y \rightarrow w$ (1,5) band.

As a check on the energy dependence of the $c'_4 \rightarrow a$ emission determined using the $c'_4 \rightarrow a$ (0,0) band we also obtained an excitation function for the $c'_4 \rightarrow a$ (0,4) band. In this case we used $p=3$ mTorr, $I=100$ μ A, and again a trapezoidal passband of 4.6 Å FWHM (the same passband dimensions as shown in Fig. 9). Correction was made for partial overlapping of the $c'_4 \rightarrow a$ (0,4) band by the violet-degraded $C^3\Pi_u \rightarrow B^3\Pi_g$ second positive (3,4) band, as well as for the continuum background, already discussed. Our $c'_4 \rightarrow a$ (0,4) band excitation function, normalized to its maximum value, is also shown in Fig. 12. The agreement between the (0,0) and (0,4) band data is good. Over the energy range $110 \leq E \leq 440$ eV, the (0,0) band data are in a constant ratio to the (0,4) band data. When these two sets of data are matched over the region $E \geq 110$ eV, the two curves are then found to differ by no more than 4% from their average over the energy range $25 \leq E \leq 110$ eV. We attribute this discrepancy between the two curves entirely to errors made in the background subtraction.

Our excitation function data shown in Fig. 12 for the $c'_4 \rightarrow a$ (0,0) and (0,4) bands includes correction for the small ($< 2.5\%$) decreases in pressure with integrated beam current, as discussed in Sec. III. However, since the total signal measured at position a (Fig. 9) is not directly proportional to pressure (see Fig. 10), we used a generalization of our correction procedure: The total signal R_c at pressure p was corrected to correspond to pressure p_0 by multiplying R_c with the factor $[1 - (1/R_c)(dR_c/dp)(p - p_0)]$. For the (0,0) and (0,4) band data shown in Fig. 12, $p_0=4$ and 3 mTorr, respectively. The value of the logarithmic derivative $(1/R)dR/dp$ at $p=p_0$ was that obtained from the total signal data used to generate the curves shown in Fig. 10. We found by experiment that, at a given pressure, the voltage dependence of the logarithmic derivative is very weak; thus, the value obtained from the signal-versus-pressure data at 200 eV, was used at all energies.

Since it was not possible for us to make meaningful polarization measurements at pressure $p < 0.1$ mTorr where the $c'_4 \rightarrow a$ signal is proportional to pressure and not affected by radiation trapping, nor was it clear what effect

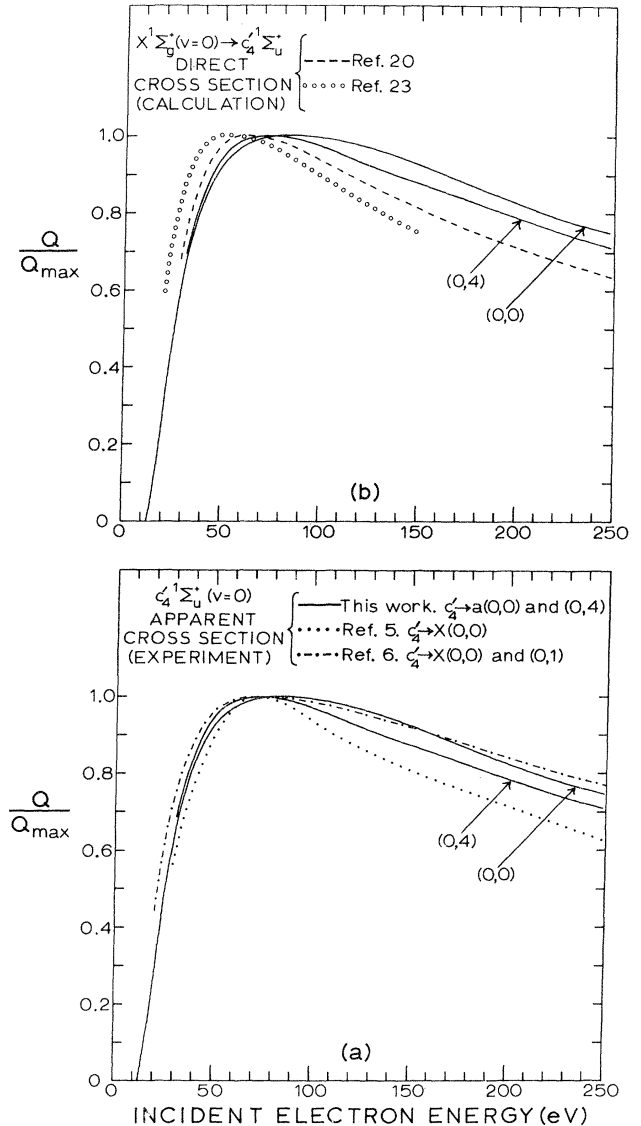


FIG. 12. (a) Comparison of energy dependence of $c'_4(0) \rightarrow a$ optical-emission data of present work (solid curves) with $c'_4(0) \rightarrow X$ data from other experiments. Present data generally lie within 3% (worst case) of the smooth solid curves. Both the (0,0) and (0,4) band results of the present work are shown here to indicate the uncertainty in our experimentally obtained curve shapes. For energies $E \geq 110$ eV, both sets of data are in constant ratio, i.e., they have same energy dependence. See Table III. When scaled by a factor of ~ 1.04 , the (0,4) band data are almost indistinguishable from the (0,0) band data for $E \geq 110$ eV and, for $25 \leq E \leq 110$ eV the two sets of data then differ by no more than $\sim 4\%$ (worst case near 30 eV) from their average. We attribute this small discrepancy between our (0,0) and (0,4) band results to error made in the background subtraction. (b) Comparison of results of present work with calculated results for $X(v=0) \rightarrow c'_4$ direct cross section.

the radiation trapping at higher pressures will have on any $c'_4 \rightarrow a$ polarization, we did not make any polarization measurements. Thus in the $c'_4 \rightarrow a$ data we have presented in Fig. 12 there is an uncertainty due to our lack of knowledge of the polarization. However, such error is

probably quite small, since the polarization determined by Ref. 6 for the $c'_4 \rightarrow X$ (0,0) and (0,1) bands was a maximum of $\sim 6\%$ near threshold and decreased to $\sim 0\%$ at 150 eV. Our correction function $Z(\mathcal{P})$ [see Eq. (7)] for the $c'_4 \rightarrow a$ (0,0) band has a value $Z \simeq 1.04$ at a polarization of 6%.

The $c'_4 \rightarrow a$ excitation function data (Fig. 12) were converted to absolute values by measuring, at 200 eV, the absolute magnitude of the (0,0) and (0,4) band optical-emission cross sections. Here we again used Eq. (7) and the same general procedures described in Sec. III. These absolute cross-section measurements were made at a manometer pressure of $p=1$ mTorr and a beam current $I=200 \mu\text{A}$ (signal was proportional to I). We corrected for the deviation of the $c'_4 \rightarrow a$ signal from linearity with pressure [see Fig. 10(a)] by reducing the cross-section measurements by a factor of 0.679. This factor is the ratio, at $p=1$ mTorr, of the dashed curve of Fig. 10(a) to the solid curve, where the solid curve is the least-squares-fitted quadratic polynomial representation of the background-corrected $c'_4 \rightarrow a$ (0,0) signal-versus-pressure measurements over the range 0–1 mTorr, and the dashed line is the linear part of the quadratic polynomial. We determined the absolute magnitude, at 200 eV, of the other cross sections of the $c'_4 \rightarrow a$ (0, v'') sequence using the measured (0,0) and (0,4) band cross sections at 200 eV and the measured branching ratios $\Gamma_{0v''}$: $Q_{\text{opt}}(0,v'') = \frac{1}{2}[(\Gamma_{0v''}/\Gamma_{00})Q_{\text{opt}}(0,0) + (\Gamma_{0v''}/\Gamma_{04})Q_{\text{opt}}(0,4)]$ for $v''=1,2,3,5$. The absolute optical-emission cross sections determined in this way at 200 eV were then scaled up to correspond to their maximum values by multiplying the values at 200 eV by the average ratio $[Q_{\text{max}}/Q(200 \text{ eV})]$ given by (0,0) and (0,4) band data of Fig. 12.

The branching ratios $\Gamma_{0v''}$ for the bands of the $c'_4 \rightarrow a$ (0, v'') sequence were also determined at 200 eV and a beam current of $I=200 \mu\text{A}$, but at a pressure of 6.5 mTorr in order to increase the precision of measurement. Although the signals were then definitely not proportional to pressure [see Fig. 10(b)], the spectral scans of the bands were all made under the same conditions of energy, pressure, and current so that cross-section ratios determined from these data will not be affected by the nonlinearity with pressure, since the cross sections all correspond to the same upper level. From the energy-level data in Ref. 15 for $c'_4^1\Sigma_u^+(v=0)$ and $a^1\Pi_g(v'')$, we expect the $c'_4 \rightarrow a$ (0,6) and (0,7) band heads to be at ~ 3877 and $\sim 4117 \text{ \AA}$, respectively. The predicted location of the (0,6) band is completely overlapped by the very intense N_2^+ first negative (1,1) band, so that we could not make any $c'_4 \rightarrow a$ (0,6) band measurements. At the predicted location of the (0,7) band we found no significant signal. Thus, in calculating the $c'_4 \rightarrow a$ branching ratios we have, with negligible error, taken $Q_{\text{opt}}(0,7)=0$ and have made a linear extrapolation with respect to v'' of the (0,4) and (0,5) band relative intensity data to obtain an approximation for the (0,6) band relative intensity. We expect this procedure to give more accurate values for the branching ratios $\Gamma_{0v''}$ for $v'' < 6$.

In Table II we give our experimental values for the maximum $c'_4 \rightarrow a$ optical-emission cross sections and the corresponding branching ratios, along with our error estimates for these quantities. In Fig. 13 are shown our normalized $c'_4 \rightarrow a$ (0,0) band data (also shown in Fig. 12) in a QE -vs- $\ln E$ plot. Figure 13 shows that above ~ 85 eV these (0,0) band data have a dependence on incident electron energy which is well described by the form $(C_1/E)\ln(E/C_2)$, where C_1 and C_2 are constants. When

TABLE II. Maximum optical-emission cross sections and branching ratios as determined in this work for bands of the $c'_4^1\Sigma_u^+(v'=0) \rightarrow a^1\Pi_g(v'')$ system of N_2 , along with our error estimates for these experimental values.

N_2 $c'_4^1\Sigma_u^+ \rightarrow a^1\Pi_g$ (0, v'')	Band head wavelength ^a (\AA)	Maximum optical-emission cross section ^b $Q_{\text{opt}}(0,v'')$ (10^{-20} cm^2)	Estimated error ^c in cross section (%)	Branching ratio $\Gamma_{0v''}$	Estimated error ^c in branching ratio (%)
(0,0)	2827.1	1.30 ^d	12	0.134 ^d	16
(0,1)	2967.0	3.16 ^e	19	0.315 ^e	16
(0,2)	3118.6	2.23 ^f	19	0.223 ^f	16
(0,3)	3283.3	1.55 ^g	22	0.155 ^g	19
(0,4)	3463.3	0.90 ^h	12	0.087 ^h	16
(0,5)	3661.1	0.59 ⁱ	22	0.058 ⁱ	19

^aReference 15, p. 220.

^bIn this work, maximum $c'_4 \rightarrow a$ signal occurred at 78.5 ± 5 eV. See Fig. 12. The (0,0) and (0,4) band cross sections were determined at 200 eV from knowledge of all quantities in Eq. (7). The other four cross sections $Q_{\text{opt}}(0,v'')$ for $v''=1,2,3,5$ were determined at 200 eV from $Q_{\text{opt}}(0,v'') = \frac{1}{2}[(\Gamma_{0v''}/\Gamma_{00})Q_{\text{opt}}(0,0) + (\Gamma_{0v''}/\Gamma_{04})Q_{\text{opt}}(0,4)]$. The maximum cross-section values listed in Table II were determined by multiplying the cross-section values at 200 eV by the factor $(0.8185)^{-1}$, where 0.8185 is the average ratio (Q/Q_{max}) at 200 eV, as given by the (0,0) and (0,4) band curves of Fig. 12.

^cThis figure obtained by adding in quadrature the estimated errors from all sources.

^dCorrected for overlapping by second positive (3,0) and Kaplan second (1,6) bands, and N^+ line $2s^22p4p^1P \rightarrow 2s2p^3^1P$ at 2823.635 \AA .

^eCorrected for overlapping by second positive (4,2), (3,1), and (2,0) bands.

^fCorrected for overlapping by second positive (3,2) band.

^gCorrected for overlapping by first negative (4,2) and (5,3) bands.

^hCorrected for contamination by unidentified atomic line at 3448.2 \AA .

ⁱCorrected for overlapping by second positive (3,5) band and unidentified atomic lines at 3636.4, 3641.6, 3643.7, 3651.3, and 3652.3 \AA .

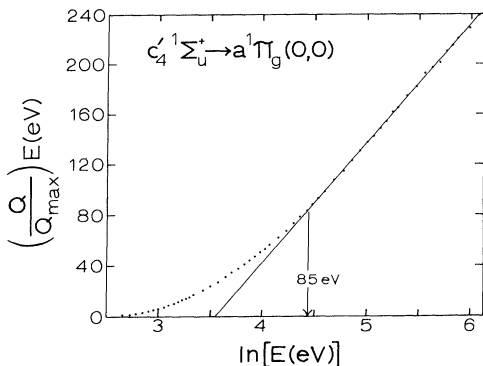


FIG. 13. QE -vs- $\ln E$ plot of the $c'_4 \rightarrow a$ (0,0) band optical-emission cross-section data of the present work, normalized to their maximum value Q_{\max} . These data are also shown as a smooth curve in Fig. 12. Above about 85 eV these $c'_4 \rightarrow a$ (0,0) band data shown in Fig. 13 are well described by the form $Q_{\text{opt}} = (C_1/E)\ln(E/C_2)$ where C_1 and C_2 are constants, with $C_2 = 34.61$ eV.

plotted in this way, our (0,4) band data above ~ 100 eV are also very well described by this form, with same C_2 value as for the (0,0) band data (see Table III). This asymptotic form of energy dependence is also expected on theoretical grounds¹⁶ for the optically allowed and spin-allowed transition $X^1\Sigma_g^+ \rightarrow c'_4^1\Sigma_u^+$ induced by electron impact.

V. DISCUSSION

A. $D^3\Sigma_u^+(v=0)$

The only band system reported in the literature for radiative decay of the $D^3\Sigma_u^+$ state of N_2 is the $D^3\Sigma_u^+ \rightarrow B^3\Pi_g$ fourth positive band system.¹⁵ Spectroscopic analysis of this band system indicates only one bound vibrational level for $D^3\Sigma_u^+$, and it has been assigned to $v=0$. Thus since the shape of the potential energy curve associated with the $D^3\Sigma_u^+$ state is not presently known, we can show only a single vibrational level in Fig. 1(a). However, the rotational constant B_0 obtained by Gerö and Schmid¹⁷ from a rotational analysis of the (0,1) and (0,2) bands yields a value of 1.10 Å for the equilibrium internuclear spacing

$r_e(D^3\Sigma_u^+)$, which turns out to be almost coincident with the r_e of 1.098 Å for the $N_2 X^1\Sigma_g^+$ ground state, and so in Fig. 1(a) we have positioned the $v=0$ level of $D^3\Sigma_u^+$ directly over the $v=0$ level of $X^1\Sigma_g^+$. The spectroscopic data for the $D \rightarrow B$ system places the $D^3\Sigma_u^+(v=0)$ level 12.84 eV above the $X^1\Sigma_g^+(v=0)$ level.¹⁵

1. Comparison with other experimental results

Our $D^3\Sigma_u^+ \rightarrow B^3\Pi_g$ optical-emission excitation-function data exhibit three noteworthy features (see Fig. 7): a primary maximum at 14.1 ± 0.3 eV, a smaller secondary maximum (83% of primary maximum) at ~ 23 eV, and a dependence on incident electron energy E which goes as E^{-3} for $E > 65$ eV. In Fig. 7 we compare our results with those of other investigators for the energy dependence of the $D \rightarrow B$ emission. The experimental data of Refs. 7 and 8 and that of the present work show some qualitative agreement in that they all exhibit two maxima, but a detailed quantitative comparison shows them not to be in good agreement. Reference 8 places the primary maximum at ~ 17.5 eV and assigns an absolute magnitude of 1.25×10^{-18} cm² at maximum for the $D^3\Sigma_u^+$ state cross section. This value is a factor of 10 larger than the value we report in Table I for the sum of the $D \rightarrow B$ optical-emission cross sections. Also, the curve of Ref. 8 is almost independent of energy for $E > 25$ eV, a result which contrasts strongly with what generally occurs for a spin-forbidden transition induced by electron impact. Since virtually no experimental detail is given in Ref. 8, we will not discuss possible reasons for the disagreement between their data and ours.

The relative intensity measurements of Ref. 7 were made at a pressure of ~ 0.005 mTorr, so that the disagreement between our data and those of Ref. 7 with respect to the energy dependence of the $D \rightarrow B$ intensity is almost certainly not due to any nonlinearity of the signal with pressure. We believe that the differences between the Ref. 7 curve and ours (see Fig. 7) may be due to three causes: (i) large spectral passband, (ii) large spread in incident electron energies, and (iii) scattered light background.

(i) As already mentioned in Sec. III, our data for the energy dependence of the $D \rightarrow B$ (0,1) band intensity were obtained using a triangular passband of FWHM ≤ 4 Å. We determined by higher-resolution investigation ($\Delta\lambda < 1$ Å

TABLE III. Values of the parameter C_2 , obtained by least-squares fitting the form $C_1 \ln(E/C_2)$ to a plot of QE vs $\ln E$ for the available experimental and theoretical works on electron-impact excitation of the $c'_4^1\Sigma_u^+$ state of N_2 .

Data	Range of data fitted (eV)	Source	C_2 (eV)
$X \rightarrow c'_4$, calculation	80–150	Reference 23	20.73
$X \rightarrow c'_4$, calculation	100–1000	Reference 20	27.67
$c'_4 \rightarrow X$ (0,1)	60–2000	Reference 4	27.89
$c'_4 \rightarrow X$ (0,0)	100–225	Reference 5	28.13
$c'_4 \rightarrow a$ (0,0)	100–2000	Reference 4	30.82
$c'_4 \rightarrow a$ (0,0)	85–440	Present work	34.61
$c'_4 \rightarrow a$ (0,4)	100–440	Present work	35.13
$c'_4 \rightarrow X$ (0,0) and (0,1)	120–300	Reference 6	40.36

FWHM) that a triangular passband of 4 \AA FWHM at position a (Fig. 5) is the largest such passband which will pick up a negligible amount of signal from the (0,0) band of the $y^1\Pi_g \rightarrow w^1\Delta_u$ Kaplan second band system.¹⁵ Reference 7 used a 25 \AA FWHM passband and, as Fig. 5 shows, a passband of this size positioned to maximize the $D \rightarrow B$ (0,1) band signal would also include a significant contribution from the Kaplan second (0,0) band. In a separate measurement, we found the Kaplan second (0,0) band has two maxima, one at $\sim 15.3 \text{ eV}$ and another at $\sim 18.3 \text{ eV}$. Inclusion of the Kaplan second (0,0) band signal will therefore tend to fill in the minimum region in the $D \rightarrow B$ signal (Fig. 7).

(ii) Second, in Ref. 7 it is stated that the data indicate an electron energy spread somewhat greater than 1 eV and a significant number of secondary electrons. Although we are not sure whether this energy spread of greater than 1 eV refers to the FWHM or the FWAB of the electron energy distribution, in either case the main effect of increasing the electron energy spread would be to make the principal maximum more rounded and smaller with respect to the secondary maximum. As mentioned in Sec. III we estimate an electron energy spread of $< 0.5 \text{ eV}$ FWAB for the electron beam used in the work we report here.

(iii) In Ref. 7 there was no mention of background correction to the excitation function. If a background correction was not made in Ref. 7, we can see another source of discrepancy between the results of Ref. 7 and ours. As explained in Sec. III, our data shown in Fig. 7 for the energy dependence of the $D \rightarrow B$ (0,1) band intensity were obtained as the *difference* of the signals at positions a and b of Fig. 5 in order to account for the energy-dependent background caused by light scattered within the monochromator. With a passband of 4 \AA FWHM, the background signal at b , as a percent of the total signal at position a , had values of $\sim 6\%$ at 14 eV , $\sim 10\%$ at 18 eV , $\sim 8\%$ at 24 eV , and $\sim 16\%$ at 40 eV . See inset curve b of Fig. 5. Because the scattered light rejection of the 0.25-m monochromator used in Ref. 7 is not as good as that for the instrument used in the present work, we would expect the background to have been an even *larger* fraction of the total signal than in the present work, and consequently, neglect of a background subtraction could have led to a significant contamination of the excitation function.

2. Maxima in the $D \rightarrow B$ optical-emission excitation function

The secondary maximum at $\sim 23 \text{ eV}$ in our $D \rightarrow B$ optical-emission excitation function (Fig. 7) can be interpreted either as due to a cascade contribution to the $D^3\Sigma_u^+(v=0)$ state population or as a feature peculiar to the direct electron-impact-excitation of the $D^3\Sigma_u^+(v=0)$ state, or perhaps as some combination of these two possibilities. In their lifetime study of the $D^3\Sigma_u^+(v=0)$ state, using the $D \rightarrow B$ (0,3) band, Kurzweg *et al.*¹¹ found that the intensity decay could be described by a simple exponential with 14-nsec decay constant. The decay mode was found to be independent of the incident electron energy.¹⁸ This finding almost completely rules out cascade as an explanation for the secondary maximum except for the very remote possibility that the cascading levels have the

same lifetime as the $D^3\Sigma_u^+(v=0)$ state. We believe that the maximum at $\sim 23 \text{ eV}$ is most likely a characteristic of the *direct* $X \rightarrow D$ electron-impact excitation. The much narrower maximum at 14.1 eV may also be an intrinsic feature of direct $D^3\Sigma_u^+(v=0)$ excitation or, it may be due to population of $D(v=0)$ via decay of a nearby resonance state. This possibility should be considered, since the available data¹⁹ indicate a Feshbach-type resonance at 14.12 eV .

3. Apparent cross section for $D^3\Sigma_u^+(v=0)$ state

The $D \rightarrow B$ optical-emission cross-section measurements we report here are for only one of the possible band systems arising from decay of the D state. The only other known state of N_2 to which the $D^3\Sigma_u^+$ state could make an optically allowed transition is the $E^3\Sigma_g^+$ state [see Fig. 1(a)]. We have found no report in the literature for the $D \rightarrow E$ band system, which would occur with wavelengths in the vicinity of $13\,500 \text{ \AA}$. The large ratio of energy differences between the D and B and the D and E states (5.47 eV and 0.94 eV , respectively) will tend to favor the $D \rightarrow B$ transition probabilities over those for $D \rightarrow E$ by a factor of $(5.47/0.94)^3 \simeq 200$. However, this could possibly be significantly offset by larger electronic transition moment and Franck-Condon factors for the $D \rightarrow E$ transition. In the absence of knowledge of the relative $D \rightarrow B$ and $D \rightarrow E$ intensity, we can say that the sum of our measured $D \rightarrow B$ optical-emission cross sections (see Table I) is a lower bound to the apparent $D^3\Sigma_u^+$ state cross section, given by the first group of terms in Eq. (4).

4. Comparison with theoretical calculation

A theoretical calculation of the direct $X \rightarrow D$ excitation cross section has been reported by Chung and Lin.²⁰ Their cross section refers to electronic excitation at the equilibrium internuclear distance of the $X^1\Sigma_g^+$ state, and, to a good approximation, is related to the direct excitation cross section for the $D^3\Sigma_u^+(v=0)$ state by the $X \rightarrow D$ (0,0) Franck-Condon factor. In Fig. 7 we compare the energy dependence of our experimental results for the $D \rightarrow B$ (0,1) band cross section with the energy dependence of the theoretical direct $X \rightarrow D$ cross section of Ref. 20. It is reasonable to make this comparison because, as we have already argued, any cascade contribution to the D state population is probably very small, and so the experimental energy dependence of the $D(v=0) \rightarrow B$ intensity should be the same as the energy dependence of the cross section for direct excitation of the $D(v=0)$ level. This calculation in Ref. 20 exhibits only *one* comparatively broad maximum at 18 eV , a result which is distinctly different from the experimental results of the present work and those of Ref. 7. The generalized oscillator strength $F(K)$ calculated in Ref. 20 for $3\sigma_g \rightarrow (3p)\sigma_u$ transitions (appropriate for calculation of the $X^1\Sigma_g^+ \rightarrow D^3\Sigma_u^+$ cross sections) is unusual, in that it has *two* maxima. This is shown in Fig. 14, which is an adaptation of Fig. 3 of Ref. 20. The two maxima in $F(K)$ suggest that two maxima in the calculated cross section might result if the second maximum in $F(K)$ were smaller with respect to the first maximum at $K=0$. Since this function $F(K)$ is determined only by the initial and final states, and it was found to be fairly insensitive to

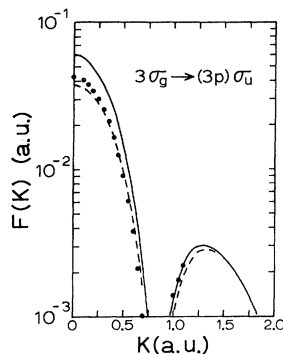


FIG. 14. Generalized oscillator strength $F(K)$ for the $3\sigma_g \rightarrow (3p)\sigma_u$ transition, appropriate to electron-impact excitation of the $N_2 D^3\Sigma_u^+$ state. Values shown here were obtained by multiplying the $G_{0n}(K)$ function calculated by Ref. 20 (and shown in Fig. 3 of Ref. 20), by the energy difference ΔE (≈ 0.4719 hartree) between $X^1\Sigma_g^+(v=0)$ and $D^3\Sigma_u^+(v=0)$. Solid line, dots, and dashed line correspond to the three wave function sets (i), (ii), and (iii), respectively, of Ref. 20. Only the function used to represent the $N_2 X^1\Sigma_g^+$ ground state is different in each calculation.

variations in the wave function used to represent the N_2 ground state $X^1\Sigma_g^+$, this suggests that a more accurate D state wave function might bring the calculation and experiment into closer agreement with regard to the energy dependence of the cross section. We are aware of only one other theoretical calculation of the direct $X \rightarrow D$ cross section, viz., that of Cartwright.²¹ The energy dependence of this calculated cross section of Ref. 21 (not shown in Fig. 7 here) also exhibits only a single maximum at ~ 17.5 eV, and is very similar to that of Ref. 20. Since only one bound vibrational level for the $D^3\Sigma_u^+$ state has been observed, it is difficult to obtain a reliable Franck-Condon factor for the $X \rightarrow D$ (0,0) transition. For this reason, we are unable to compare the absolute magnitude of the calculations of Refs. 20 and 21 with the experimental results of the present work for the $D(0) \rightarrow B$ optical-emission cross section.

5. Comparison of $D \rightarrow B$ and $C \rightarrow B$ optical-emission cross sections

Our measured maximum optical-emission cross section for the $D \rightarrow B$ band system is less than 0.3% of the maximum optical-emission cross section determined by Jobe, Sharpton, and St. John²² for the $C^3\Pi_u \rightarrow B^3\Pi_g$ second positive band system of N_2 which also reaches a maximum at ~ 14 eV. Thus the $D^3\Sigma_u^+ \rightarrow B^3\Pi_g$ fourth positive band system contribution to the B state population is negligible in comparison with the $C^3\Pi_u \rightarrow B^3\Pi_g$ second positive band system contribution. This also shows that the indirect D state contribution to the metastable $A^3\Sigma_u^+$ state population via $D \rightarrow B \rightarrow A$ is negligible with respect to the $C \rightarrow B \rightarrow A$ contribution.

B. $c'_4 \ ^1\Sigma_u^+(v=0)$

Our experimental results for the energy dependence of the $c'_4 \rightarrow a$ intensity are characterized by a single, very

broad maximum in the vicinity of 80 eV, and for $E > 110$ eV, $Q_{\text{opt}}(c'_4 \rightarrow a) \approx (C_1/E)\ln(E/C_2)$.

1. Comparison of energy dependence of $c'_4 \rightarrow a$ emission with other experimental work and with theoretical calculation

In Fig. 12 we compare our data for the energy dependence of the $c'_4 \rightarrow a$ (0,0) and (0,4) band optical-emission cross section with the experimental results of Refs. 5 and 6, in which the $c'_4 \rightarrow X(0, v'')$ bands were used. We also show the energy dependence of the cross section for direct electron-impact excitation of all levels of the c'_4 state, as calculated by Chung and Lin²⁰ and by Hazi.²³ Each set of data shown in Fig. 12 has been normalized to its maximum value. The data of Refs. 5 and 6 and that of the present work should all exhibit precisely the same energy dependence since they all correspond to decay of a common upper level, $c'_4 \ ^1\Sigma_u^+(v=0)$. As Fig. 12 shows, however, there are some disagreements between our experimental results and those of Refs. 5 and 6. The data of both Refs. 5 and 6 reach a maximum near 71 eV, while our $c'_4 \rightarrow a$ (0,0) band data have a maximum near 83 eV. Our disagreement with the results of the other investigators for the location of the maximum may be due to errors made in our background subtraction since our $c'_4 \rightarrow a$ (0,4) band data, also shown in Fig. 12, reach a maximum near 75 eV. Of the experimental data, that of Ref. 6 and the (0,0) band data of the present work show the closest agreement.

Each curve in Fig. 12 [and also the data of Ref. 4 for $c'_4 \rightarrow X(0,1)$, which are not shown in Fig. 12] exhibits, at higher energies, an energy dependence described by the form $(C_1/E)\ln(E/C_2)$, where C_1 and C_2 are constants. This form has also been derived theoretically.²⁴ In the theoretical derivation, the parameter C_2 is determined only by the functional dependence on K of the generalized oscillator strength $F(K)$, and the energy difference between the initial and final molecular states. In Fig. 13 we illustrate how the $c'_4 \rightarrow a$ (0,0) band data of the present work reach this asymptotic form of energy dependence, and we give in Table III the value of the constant C_2 which we have derived from each of the available experimental and theoretical works. As Table III shows, our data for the $c'_4 \rightarrow a$ (0,0) and (0,4) bands are self-consistent, in that the values of the constant C_2 obtained from these data are within ± 0.3 eV of their mean value. The values of C_2 obtained from the data of Refs. 4 and 5 and the calculation of Ref. 20, which differ from their mean value by no more than ± 0.2 eV, have a mean value which is 7 eV smaller than the mean value of C_2 obtained from our data. The smallest and largest values of C_2 are given by the calculation of Ref. 23 and the data of Ref. 6, respectively. Since cascade contributions to the population of $c'_4 \ ^1\Sigma_u^+(v=0)$ can alter the constants in the asymptotic form $(C_1/E)\ln(E/C_2)$ describing the energy dependence of emission from the $c'_4(v=0)$ state, then one must be careful in comparing the C_2 values obtained from experimental data, with the values obtained from theoretical calculations of the direct $X \rightarrow c'_4$ cross section. However, if the form $(C_1/E)\ln(E/C_2)$ truly describes the energy dependence of the emission from $c'_4(v=0)$ at higher energies, then differences in slope of the QE -vs- $\ln E$ plots are expected because of differences in scaling of the data, but

all the experimental data should yield the same value for the intercept C_2 , in the QE -vs- $\ln E$ plots. We have not found a plausible explanation for the variety of C_2 values given by the experimental data.

2. Comparison of $c_4^1(0) \rightarrow a$ and $c_4^1(0) \rightarrow X$ optical-emission cross sections

From the sum of our measured optical-emission cross sections for the $c_4^1\Sigma_u^+ \rightarrow a^1\Pi_g(0, v'')$ bands (see Table II) and the absolute cross sections for the $c_4^1 \rightarrow X(0, 0)$ and $(0, 1)$ bands measured by Refs. 5 and 4, respectively, we obtain an *upper bound* of $\Gamma \leq 0.006$ for the $c_4^1\Sigma_u^+(v=0) \rightarrow a^1\Pi_g$ optical branching ratio [i.e., $\Gamma \geq 0.994$ for $c_4^1\Sigma_u^+(v=0) \rightarrow X^1\Sigma_g^+$]. In this estimated upper bound for the $c_4^1(0) \rightarrow a$ branching ratio, we are ignoring the $c_4^1(0) \rightarrow a''$ branching, where $a''^1\Sigma_g^+$ is the only other known singlet state to which $c_4^1\Sigma_u^+$ can decay.¹⁵ The band system arising from the transition $c_4^1\Sigma_u^+ \rightarrow a''^1\Sigma_g^+$ (this is the singlet analog of the $D^3\Sigma_u^+ \rightarrow E^3\Sigma_g^+$ system) will occur with wavelengths in the vicinity of $1.8 \mu\text{m}$. See Fig. 1(b). We have found no report in the literature for this band system and just as in the case of the $D \rightarrow E$ system we expect such a system to be very weak with respect to the $c_4^1 \rightarrow a$ system. Thus since the $c_4^1 \rightarrow a$ optical-emission cross sections are so small with respect to the $c_4^1 \rightarrow X$ cross sections, taking into account the probably even smaller $c_4^1 \rightarrow a''$ optical-emission cross sections will make no significant change in the estimate of the $c_4^1 \rightarrow a$ branching ratio.

3. Effect of $c_4^1(v=0) \rightarrow a^1\Pi_g$ cascade on a $^1\Pi_g \rightarrow X$ emission

The marked nonlinearity in the pressure dependence of the $c_4^1(0) \rightarrow a$ emission (see Fig. 10) implies a nonlinear-with-pressure cascade contribution to the $a^1\Pi_g$ population. In a study of electron-impact excitation of bands of the $a^1\Pi_g \rightarrow X^1\Sigma_g^+$ Lyman-Birge-Hopfield system,¹⁵ Holland²⁵ observed nonlinearities with pressure similar to what we shown in Fig. 10. In Holland's work, the dependence on pressure p of the intensity of the $a \rightarrow X$ bands was fairly well described by the quadratic form $ap + bp^2$ over the pressure range $0.03 \leq p \leq 0.9$ mTorr, with significant (5%) deviation from linearity with the pressure being evident even at $p=0.1$ mTorr for emission from the $a^1\Pi_g(v=0)$ level. The ratio (b/a) of the coefficients depended on the vibrational level v of $a^1\Pi_g$. It was largest for emission from $a^1\Pi_g(v=0)$, and decreased for increasing v , with $b/a \approx 0$ for emission from $a^1\Pi_g(v=5, 6)$. No emission was observed from $a^1\Pi_g(v)$ for $v > 6$. Holland reported that the observed pressure dependence of the $a \rightarrow X$ band intensities, measured at incident electron energies of 200, 900, and 1800 eV was very similar. Aarts and DeHeer,⁴ who studied the pressure dependence of the $a \rightarrow X(2, 0)$ band at 60 and 600 eV found nonlinearity with pressure also described by the form $ap + bp^2$, with the ratio (b/a) at 600 eV being about twice as large as at 60 eV. In their paper, Aarts and DeHeer argued that the cascade contribution to $a^1\Pi_g(v)$ from the $c_4^1 \rightarrow a(0, v)$ bands is a probable cause of the complicated deviation from linearity

with pressure seen in the $a \rightarrow X$ bands: The relative amount of cascade contribution to the different vibrational levels v of $a^1\Pi_g$ will depend on v because of the different branching ratios Γ_{0v} for the $c_4^1 \rightarrow a(0, v)$ bands. The nonlinearity with pressure will have some energy dependence because the cross sections for direct excitation of $a^1\Pi_g$ and $c_4^1\Sigma_u^+$ have different magnitude and energy dependence. However, as we show in Table IV, the $c_4^1 \rightarrow a(0, v)$ optical emission alone appears to be too small to account for all the observed nonlinearity in the pressure dependence of the $a \rightarrow X$ band intensities. In column 4 of Table IV we show the nonlinearity for the $a \rightarrow X$ bands at 900 eV as given by Holland's data (Fig. 5 of Ref. 25). This nonlinearity is expressed as the ratio (b/a) of the coefficients in the quadratic form $ap + bp^2$ describing the pressure dependence of the integrated band intensities. In column 5 we give the expected nonlinearity in the $a \rightarrow X$ bands assuming it is due entirely to cascade and $c_4^1 \rightarrow a(0, v)$ is the only cascade into $a^1\Pi_g(v)$. Our estimate is based upon the absolute cross-section data of Holland for the $a \rightarrow X$ bands, the $c_4^1 \rightarrow a$ cross-section data of the present work, and the deviation from linearity with the pressure over the range 0–1 mTorr for the $c_4^1 \rightarrow a$ emission as determined in the present work [see Fig. 10(a)]. The nonlinearity in the $c_4^1 \rightarrow a(0, 0)$ band signal-versus-pressure data of the present work (Fig. 10) is characterized by a value 0.472 for the coefficient ratio (b/a). Even allowing for $\pm 20\%$ error in both the cross-section data of Holland and of the present work, the predicted nonlinearity is never more than 10% of the observed. Also, the nonlinearity in the $a \rightarrow X$ data is largest for $a^1\Pi_g(v=0)$, while we found the $c_4^1 \rightarrow a(0, v)$ cascade largest for $v=1$. If nonlinear-with-pressure cascade into $a^1\Pi_g$ is the sole cause of the observed nonlinearity with pressure in the $a \rightarrow X$ bands, then the results given in column 5 of Table IV indicate the existence of a much larger nonlinear-with-pressure cascade contribution to the $a^1\Pi_g$ levels than is provided by the $c_4^1 \rightarrow a(0, v)$ bands alone. Zipf and McLaughlin⁵ have measured optical-emission cross sections at 200 eV for bands of the $(b', c', e')^1\Sigma_u \rightarrow X^1\Sigma_g^+$ and $(b, c, e, o)^1\Pi_u \rightarrow X^1\Sigma_g^+$ systems. These valence- and Rydberg-type states can also branch to the $a^1\Pi_g$ state. See Table 20 of Ref. 15. Since these $^1\Sigma_u$ and $^1\Pi_u$ states are optically connected to the ground state, then we would expect all the $^1\Sigma_u \rightarrow a^1\Pi_g$ and $^1\Pi_u \rightarrow a^1\Pi_g$ bands to exhibit nonlinearity with pressure similar to that observed in the $c_4^1 \rightarrow a$ bands. The measurements of Ref. 5 indicate that the total optical-emission cross section at 200 eV ($2.2 \times 10^{-17} \text{ cm}^2$) for all the $^1\Sigma_u \rightarrow X$ and $^1\Pi_u \rightarrow X$ transitions of these $^1\Sigma_u$ and $^1\Pi_u$ states which lie between 12.5 and 15 eV, is only twice as large as the optical-emission cross section for $c_4^1\Sigma_u^+ \rightarrow X^1\Sigma_g^+(0, 0)$ alone. If we assume that the vibrational levels of these $^1\Sigma_u$ and $^1\Pi_u$ states have branching ratios to the $a^1\Pi_g$ state which are close to the value 0.006 we have determined for the $c_4^1(v=0) \rightarrow a$ transitions and if we assume that the $^1\Sigma_u \rightarrow a^1\Pi_g$ and $^1\Pi_u \rightarrow a^1\Pi_g$ bands exhibit the same nonlinear pressure dependence we have observed in the case of the $c_4^1 \rightarrow a(0, v)$ bands, then this still can explain only a small part of the observed nonlinear pressure dependence of the $a \rightarrow X$ bands. This discrepancy suggests that the cascade contri-

TABLE IV. Comparison of observed and predicted nonlinearity in pressure dependence of $a^1\Pi_g \rightarrow X^1\Sigma_g^+(v, v')$ band intensity.

v	Present work	Holland, Ref. 25		Predicted
	$Q_{\text{opt}}[c'_4 \rightarrow a(0, v)]^a$ at 900 eV (10^{-20} cm 2)	$Q_{\text{app}}[a^1\Pi_g(v)]^b$ at 900 eV (10^{-20} cm 2)	b/a^c at 900 eV (mTorr $^{-1}$)	b/a^d at 900 eV (mTorr $^{-1}$)
0	0.439	5.36	0.647	0.036
1	1.069	14.50	0.502	0.032
2	0.755	21.19	0.306	0.016
3	0.526	22.81	0.163	0.011
4	0.303	27.77	0.093	0.005
5	0.196	28.90	0.000	0.003

^aThese values were obtained from the $c'_4 \rightarrow a$ optical-emission cross sections of the present work, measured at 200 eV, and the asymptotic form $(C_1/E)\ln(E/C_2)$ for the energy dependence of the $c'_4 \rightarrow a$ optical-emission cross sections for $E > 200$ eV. In this extrapolation, we have used $C_2 = 34.87$ eV, which is the average of the C_2 values determined in the present work for the $c'_4 \rightarrow a(0,0)$ and $(0,4)$ bands. See Table III.

^b $Q_{\text{app}}[a^1\Pi_g(v)] = \sum_v Q_{\text{opt}}[a \rightarrow X(v, v')]$ is the apparent cross section for exciting vibrational level v of $a^1\Pi_g$. The $a \rightarrow X(v, v')$ optical-emission cross sections were obtained from Holland's best value of $(1.1 \pm 0.2) \times 10^{-18}$ cm 2 for exciting the entire $a \rightarrow X$ system with 900-eV electrons and the calculated fractions $f_{w'}$ given in Holland's Table I, i.e., $Q_{\text{opt}}[a \rightarrow X(v, v')] = (1.1 \times 10^{-18} \text{ cm}^2) f_{w'}$ at 900 eV.

^cNonlinearity in signal-vs-pressure data of Holland for $a \rightarrow X(v, v')$ bands at 900 eV, expressed as the ratio (b/a) of coefficients in the quadratic form $ap + bp^2$ describing the pressure dependence of the data over the range $0.03 \leq p \leq 0.9$ mTorr. See Fig. 5 of Holland.

^dPredicted ratio (b/a) assuming the nonlinear-with-pressure $c'_4 \rightarrow a(0, v)$ intensity is the only cascade source for $a^1\Pi_g(v)$. This predicted ratio is given by $(Q_{\text{opt}}[c'_4 \rightarrow a(0, v)] / \{Q_{\text{dir}}[a^1\Pi_g(v)] + Q_{\text{opt}}[c'_4 \rightarrow a(0, v)]\}) (b/a)^*$ where $(b/a)^* = 0.4718$ characterizes the nonlinearity with pressure in the $c'_4 \rightarrow a(0, v)$ emission, as determined in the present work over the pressure range $0 \leq p \leq 1$ mTorr [see Fig. 10(a)]. In this calculation we have taken $Q_{\text{dir}}[a^1\Pi_g(v)] \approx Q_{\text{app}}[a^1\Pi_g(v)]$ because $Q_{\text{opt}}[c'_4 \rightarrow a(0, v)]$ is small with respect to $Q_{\text{app}}[a^1\Pi_g(v)]$. Compare columns 2 and 3 of Table IV.

tribution to $a^1\Pi_g$ from these other $^1\Sigma_u$ and $^1\Pi_u$ states may be much larger (say 4 or 5 times larger) than the contribution from $c'_4(v=0) \rightarrow a$ alone. This does not seem very likely, however: Our survey spectral scans of the region 2600–3700 Å indicate that the intensities of the other bands of the $^1\Sigma_u \rightarrow a$ and $^1\Pi_u \rightarrow a$ Gaydon-Herman singlet systems are smaller collectively, than for the $c'_4(v=0) \rightarrow a$ bands. Since the $a^1\Pi_g$ state is metastable ($\bar{\tau} \sim 115$ msec), molecule-molecule collisional shortening of the lifetime may be a more likely source of the pressure nonlinearity in the $a \rightarrow X$ radiation. Further experimental investigation is needed to clear up this point.

C. Nonlinearities in pressure and current dependence of the $D \rightarrow B$ and $c'_4 \rightarrow a$ signals

For both the $D \rightarrow B$ and $c'_4 \rightarrow a$ signals the deviation from linearity with the beam current (see Secs. III and IV) was largest for energies in the vicinity of 30 eV, but in opposite senses: As the current was increased at constant accelerating voltage and pressure, the $D \rightarrow B$ signal increased less strongly with current and the $c'_4 \rightarrow a$ signal increased more strongly with current than expected from a simple proportional extension of the low-current data. We have been unable to understand this apparent energy-dependent nonlinearity in the signal-versus-current data.

The very nonlinear pressure dependence of the emission from the c'_4 state we have already discussed in Sec. IV. In the case of the energy-dependent nonlinear pressure

dependence of the $D \rightarrow B$ signal (see Fig. 6) we offer the following speculative and qualitative explanation: At a given accelerating voltage, pressure, and total current $I = (I_8 + I_9 + I_{11})$, the flux of electrons through the viewed region about point P (Fig. 2) will consist of an approximately monoenergetic component of electrons which have traveled from the cathode K to P without making a collision, plus a smaller component consisting of electrons which have made one or more inelastic collisions before reaching P or have been inelastically backscattered after traveling past P . Electrons ejected in ionizing collisions (both to left and to right of P) will also contribute to the flux through the region about P . Experimental evidence supports this picture. The current to electron-gun element 8 (see Fig. 2) must be collected almost entirely by the surface of element 8 which faces into the interior of the Faraday cup formed by elements 9 and 11, because the other side of element 8 is masked by element 7. This masking of element 8 by element 7 means that the current I_8 should have no direct contribution from the primary beam and thus will be due mainly to backscattered and ejected electrons from the region to the right of element 8 in Fig. 2. There could be a contribution to I_8 from positive ions N_2^+ and N^+ produced by dissociative excitation of N_2 , but I_8 is found to be negative (in the sense of electron flow to element 8) so that the electron contribution dominates. Individual measurements of the currents show that the current I_8 increases with pressure at constant current I

and energy, and $I_8 \propto I$ at constant energy ($E < 20$ eV) and constant pressure ($p < 5$ mTorr). At fixed current I and pressure, I_8 decreases as we raise the energy. For example, at $I = 10.00 \mu\text{A}$ and $p = 3$ mTorr, $I_8 = 0.60 \mu\text{A}$ at 15 eV, $I_8 = 0.55 \mu\text{A}$ at 25 eV, and $I_8 = 0.48 \mu\text{A}$ at 50 eV. We suppose this smaller, pressure-dependent component of the electron flux to have an energy distribution strongly favoring low energies. As we raise the energy, the $D \rightarrow B$ intensity due to direct excitation of the D state by the primary component of the electron flux decreases quickly with energy for $E > 25$ eV (see Fig. 7), and the $D \rightarrow B$ signal due to excitation of the D state by the pressure-dependent low-energy component of the flux becomes an increasing fraction of the total $D \rightarrow B$ signal because the low-energy electrons are much more effective in exciting the D state. In this way then, a given deviation of the $D \rightarrow B$ signal from proportional dependence on pressure would occur at lower pressure as we raise the energy.

VI. SUMMARY

Production of the $D^3\Sigma_u^+(v=0) \rightarrow B^3\Pi_g$ fourth positive band system by electron-impact excitation of N_2 molecules in the $X^1\Sigma_g^+(v=0)$ ground state has three characteristic features: A principal maximum at 14.1 ± 0.3 eV where the $D(v=0) \rightarrow B$ optical-emission cross section reaches a value $1.3 \times 10^{-19} \text{ cm}^2$, a smaller maximum (83% of principal maximum) at 23 eV, and an E^{-3} energy dependence for incident electron energies $E > 65$ eV. The $D \rightarrow B$ radiation is unpolarized. Significant radiative cascade contribution to the $D^3\Sigma_u^+(v=0)$ state population is very unlikely. The maximum at ~ 23 eV is most likely a characteristic feature of the $X^1\Sigma_g^+(v=0) \rightarrow D^3\Sigma_u^+(v=0)$ cross section. The narrower maximum at ~ 14.1 eV may also be an intrinsic feature of the $X \rightarrow D$ excitation or, it may be due to population of $D(v=0)$ via decay of a resonance. The two maxima in the $D \rightarrow B$ optical-emission

cross section contrast markedly with the existing theoretical calculations for the direct $X \rightarrow D$ cross section, which exhibit only a single maximum. Additionally, the results of the present work show that the cascade contribution of the $D^3\Sigma_u^+$ state to the population of the $B^3\Pi_g$ and the metastable $A^3\Sigma_u^+$ states of N_2 via $D \rightarrow B$ and $D \rightarrow B \rightarrow A$, respectively, is quite small ($< 0.3\%$) with respect to the contribution from the N_2 $C^3\Pi_u$ state via $C \rightarrow B$ and $C \rightarrow B \rightarrow A$.

Production of the $c'_4{}^1\Sigma_u^+(v=0) \rightarrow a^1\Pi_g$ Gaydon-Herman singlet system by electron-impact excitation of N_2 molecules in the $X^1\Sigma_g^+(v=0)$ ground state is characterized by a single very broad maximum near 80 eV, where the $c'_4(v=0) \rightarrow a$ optical-emission cross section reaches a value $1.0 \times 10^{-19} \text{ cm}^2$; for $E > 110$ eV, the energy dependence of the $c'_4(v=0) \rightarrow a$ optical-emission cross section is described by the form $(C_1/E)\ln(E/C_2)$, where C_1 and C_2 are constants. Target gas densities corresponding to pressures < 0.1 mTorr must be used to avoid significant nonlinearity with pressure in the $c'_4(v=0) \rightarrow a$ signal caused by trapping of $c'_4 \rightarrow X(0,0)$ band radiation. The $c'_4(v=0) \rightarrow a$ optical branching ratio is very small (< 0.006) compared with the $c'_4(v=0) \rightarrow X$ branching ratio (> 0.994). The results of the present work also show that the pressure-enhanced cascade contribution from the $c'_4(v=0) \rightarrow a$ bands to the population of $a^1\Pi_g$ molecules can explain only a very small part ($\sim 10\%$) of the observed nonlinearity with pressure in the $a \rightarrow X$ Lyman-Birge-Hopfield bands.

ACKNOWLEDGMENTS

This work was supported by the U.S. Air Force Office of Scientific Research. The authors thank Dr. R. S. Freund for reading and commenting on the manuscript.

¹See, for example, D. R. Bates, in *Physics of the Upper Atmosphere*, edited by J. A. Ratcliffe (Academic, New York, 1960), Chap. 7, pp. 297–353; A. E. S. Green and C. A. Barth, *J. Geophys. Res.* **70**, 1083 (1965); R.S. Stolarski and A. E. S. Green, *ibid.* **72**, 3967 (1967); V. Degen, *J. Quant. Spectrosc. Radiat. Transfer* **18**, 113 (1977).

²P. K. Carroll and K. Yoshino, *J. Chem. Phys.* **47**, 3073 (1967).

³See, for example, H. Lefebvre-Brion, and C. M. Moser, *J. Chem. Phys.* **43**, 1394 (1965).

⁴J. F. M. Aarts and F. J. DeHeer, *Physica (Utrecht)* **52**, 45 (1971).

⁵E. C. Zipf and R. W. McLaughlin, *Planet. Space Sci.* **26**, 449 (1978).

⁶J. C. Huschilt, H. W. Dassen, and J. W. McConkey, *Can. J. Phys.* **59**, 1893 (1982).

⁷R. S. Freund, *J. Chem. Phys.* **54**, 1407 (1971).

⁸V. V. Skubenich and I. P. Zapesochny, in *Abstract of Papers, Fifth International Conference on the Physics of Electronic and Atomic Collisions, Leningrad, U.S.S.R., 1967* (Nauka, Leningrad, 1967), p. 570.

⁹To reduce the effect on electron trajectories caused by the magnetic field of the earth and a nearby ion pump magnet, the

electron gun was enclosed by a coaxial 26-cm-long, 9.5-cm-diameter open-ended cylinder of 0.64-mm-thick Conetic AA magnetic shielding alloy (a product of Perfection Mica Corporation). Measurements showed that on the axis XX' , over a range of ± 8 cm about point P , the shielding cylinder reduced the magnitude of the field component perpendicular to XX' by a factor of ~ 10 , to a value of $B_1 < 0.05$ G.

¹⁰Tests using a set of eight such slits with widths varying from 0.4 to 2.5 mm showed that the photomultiplier signal currents developed using such an irradiance source were directly proportional to the slit width w .

¹¹L. Kurzweg, G. T. Egbert, and D. J. Burns, *J. Chem. Phys.* **59**, 2641 (1973).

¹²J. E. Hesser and K. Dressler, *J. Chem. Phys.* **45**, 3149 (1966).

¹³MKS Instruments, Inc., Burlington, Massachusetts. Model 310-BHS-1 absolute pressure transducer.

¹⁴In a test using the (0,0) band of the N_2^+ first negative system as a signal source, we found that for a given pressure reading p , over the range 0–11 mTorr, there was $< 0.5\%$ difference between the signals developed with the transducer at room temperature (297 K) and with the transducer at its normal operating temperature of 318 K. See M. C. I. Siu, *J. Vac. Sci.*

- Technol. 10, 368 (1973), for a formal treatment of the thermal transpiration effect.
- ¹⁵A. Lofthuis and P. H. Krupenie, *J. Phys. Chem. Ref. Data* 6, 113 (1977).
- ¹⁶See, for example, M. Inokuti, *Rev. Mod. Phys.* 43, 325 (1971).
- ¹⁷L. Gerö and R. Schmid, *Z. Phys.* 116, 598 (1940).
- ¹⁸D. L. Burns (private communication). We thank Dr. Burns for providing us with this information and for helpful conversation.
- ¹⁹See, for example, G. J. Schulz, *Rev. Mod. Phys.* 45, 423 (1973). The present situation may be similar to the case of electron-impact excitation of the $N_2 E^3\Sigma_g^+(v=0)$ state (11.87 eV) in which the very sharp rise of the cross section at threshold has been attributed to an N_2^- state at 11.92 eV [J. R. Mazeau, R. I. Hall, G. Joyez, M. Landau, and J. Reinhardt, *J. Phys. B* 6, 873 (1973)].
- ²⁰S. Chung and C. C. Lin, *Phys. Rev. A* 6, 988 (1972).
- ²¹D. C. Cartwright, *Phys. Rev. A* 2, 1331 (1970).
- ²²J. D. Jobe, F. A. Sharpton, and R. M. St. John, *J. Opt. Soc. Am.* 57, 106 (1967).
- ²³U. A. Hazi, *Phys. Rev. A* 23, 2232 (1981).
- ²⁴This asymptotic form for the energy dependence of the cross section is the first term in a series expansion in powers of $1/E$ derived by Bethe [H. Bethe, *Ann. Phys. (Leipzig)* 5, 325 (1930)]. The constant C_2 is determined by the generalized oscillator strength for the collisional excitation.
- ²⁵R. F. Holland, *J. Chem. Phys.* 51, 3940 (1969).